# TECHNICAL REPORT No. 43

## A NEW CONVECTIVE ADJUSTMENT SCHEME

## PART I: OBSERVATIONAL AND THEORETICAL BASIS

by

A.K. Betts*

## PART II: SINGLE COLUMN TESTS USING GATE-WAVE, BOMEX, ATEX AND ARCTIC AIRMASS DATA SETS

by

A.K. Betts* and M.J. Miller

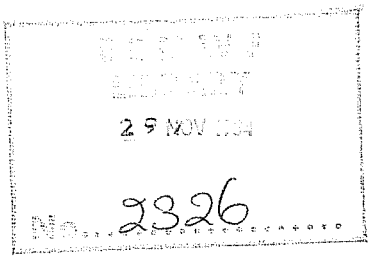


* Visiting Scientist

October 1984

## A B S T R A C T

A new convective adjustment scheme is proposed, based on the simultaneous adjustment of temperature and moisture fields towards observed quasi-equilibrium thermodynamic structures, with an adjustment time lag of order two hours. Separate schemes are used for deep and shallow (non-precipitating) convection.

The schemes are tested using single column data sets from tropical field experiments (GATE, BOMEX, ATEX) and an Arctic airmass transformation. Preliminary global forecasts show significant improvements in the global surface fluxes and mean tropical temperature tendency over the operational Kuo convection scheme.

# A NEW CONVECTIVE ADJUSTMENT SCHEME

## PART I: OBSERVATIONAL AND THEORETICAL BASIS

by

**A. K. Betts**

CONTENTS PAGE


1. INTRODUCTION 2

2. OBSERVATIONAL BASIS 4

2.1 Deep convection 4

2.1.1 Convective soundings over the tropical ocean 4
2.1.2 Convective equilibrium over land 6
2.1.3 Fast moving storms over land 11
2.1.4 Deep convective equilibrium structure: parametric philosophy 11

2.2 Shallow convection 18

2.2.1 Mixing line structure 18
2.2.2 Trade cumulus equilibrium 18

3. CONVECTIVE ADJUSTMENT SCHEME 19

3.1 Formal structure 20

3.2 Adjustment procedure 21

3.3 Reference thermodynamic profiles 22
3.3.1 Deep convection reference profile 23
3.3.2 Shallow convection reference profile 25

4. CONCLUDING REMARKS 26

## 1. INTRODUCTION

Cumulus parameterisation started with simple attempts to represent the subgrid-scale effects of convective clouds. Manabe et al.(1966) proposed adjustment towards a moist adiabatic structure in the presence of conditional instability, and Kuo (1965, 1974) proposed a simple cloud model to redistribute the heating and moistening effects of precipitating clouds in the presence of grid scale moisture convergence. The work of Ooyama (1971), and Arakawa and Schubert (1974) initiated a great deal of research attempting to parameterise cloud ensembles using a cloud spectrum and a simple cloud model (see review by Frank (1983)). One of the key objectives of the GATE experiment (Betts, 1974) was to study organised deep convection in the tropics to test and develop convective parameterisations for numerical models. GATE diagnostic studies have documented the complexity of tropical mesoscale convection (Houze and Betts, 1981): from the importance of mesoscale updrafts and downdrafts as well as convective-scale processes down to the effects of the cloud microphysical processes of freezing, melting and water loading. One might conclude from these phenomenological studies that cloud models of much greater complexity might be needed to parameterise cumulus convection (Frank, 1983). Little progress has been made in this direction, however, because it is clearly impossible to attempt to integrate at each grid-point in a global model, a cloud-scale model of much realism.

This paper represents a marked divergence in philosophy: the primary objective of the proposed parameterisation scheme (Betts, 1983b) is to ensure that the local vertical temperature and moisture structure in the large-scale model, which in nature are strongly constrained by convection, be realistic. The

concept of a quasi-equilibrium between the cloud field and the large-scale forcing (introduced by Betts (1973) for shallow convection and Arakawa and Schubert (1974) for deep clouds) has been well-established, at least on larger space and time scales (Lord and Arakawa, 1980; Lord, 1980, 1982). This means that convective regions have characteristic temperature and moisture structures which can be documented observationally, and used as the basis of a convective adjustment procedure. Betts (1973) and Albrecht et al (1979) modelled shallow convection using this approach. The main limitation of the moist adiabatic convective adjustment suggested by Manabe et al (1966) for deep convection is that the tropical atmosphere does not approach a moist adiabatic equilibrium structure in the presence of deep convection. In the scheme proposed here we shall adjust simultaneously the temperature and moisture structure towards observed quasi-equilibrium structures. This ensures that on the grid-scale a global model always maintains a realistic vertical temperature and moisture structure in the presence of convection. This sidesteps all the details of how the subgrid-scale cloud and meso-scale processes maintain the quasi-equilibrium structures we observe. To the extent that one can show observationally that different convective regions have different quasi-equilibrium thermodynamic structures (as a function of wind-field for example), these could be incorporated using different adjustment parameters. However, in this paper we introduce just the simplest scheme to show its usefulness.

We shall use the saturation point formulation of moist thermodynamics (Betts, 1982a) to introduce the observational and theoretical basis of the proposed convective adjustment. We then apply the scheme (Part II) to a series of data sets from GATE, BOMEX, ATEX and an Arctic air-mass transformation to show the sensitivity of the scheme to different parameters, and develop a parameter set

suitable for both shallow and deep convection in a global model. Part III (in preparation) will show the effect of the scheme on global forecasts.

## 2. OBSERVATIONAL BASIS

Betts (1982a) has given examples of deep and shallow convective equilibrium structures, and Betts (1983a) has discussed equilibrium structure for mixed cumulus layers. Here we present a few examples, which inspired the parameterization scheme. We shall present tephigrams showing temperature and saturation point ((T, p) at the lifting condensation level: abbreviated SP). Isopleths of virtual potential temperature ($\theta_{ESV}$) for cloudy air will be shown for reference (Betts, 1983), together with $\mathcal{P}$, the pressure departure of air at each pressure level from its saturation level.

### 2.1 Deep convection

#### 2.1.1 Convective soundings over the tropical ocean

Fig. 1.1 shows an extreme example: the structure of the deep troposphere for the mean typhoon sounding from Frank (1977). The heavy dots and open circles are temperature and saturation point (T, SP) for the eyewall. They show a temperature structure which parallels a $\theta_{ESV}$ isopleth below 600 mb and $\theta_{ES}$ increasing above, with a nearly saturated atmosphere ($p_{sl}-p = \mathcal{P} = -15$ mb). The crosses and symbols E are (T, SP) inside the eyewall. Here the strong subsidence has produced a very stable thermal structure, but the SP structure is very close to the temperature structure of the eyewall: it has been generated by subsidence of air originally saturated at the eyewall temperature (this does not modify the SP). The mid-tropospheric subsidence within the eye (of this composite) is 60 mb. Thus the temperature structure of the eyewall is confirmed by two independent composites. Even in this extreme case of strong convection in a typhoon, the mean temperature structure is quite far from moist adiabatic.

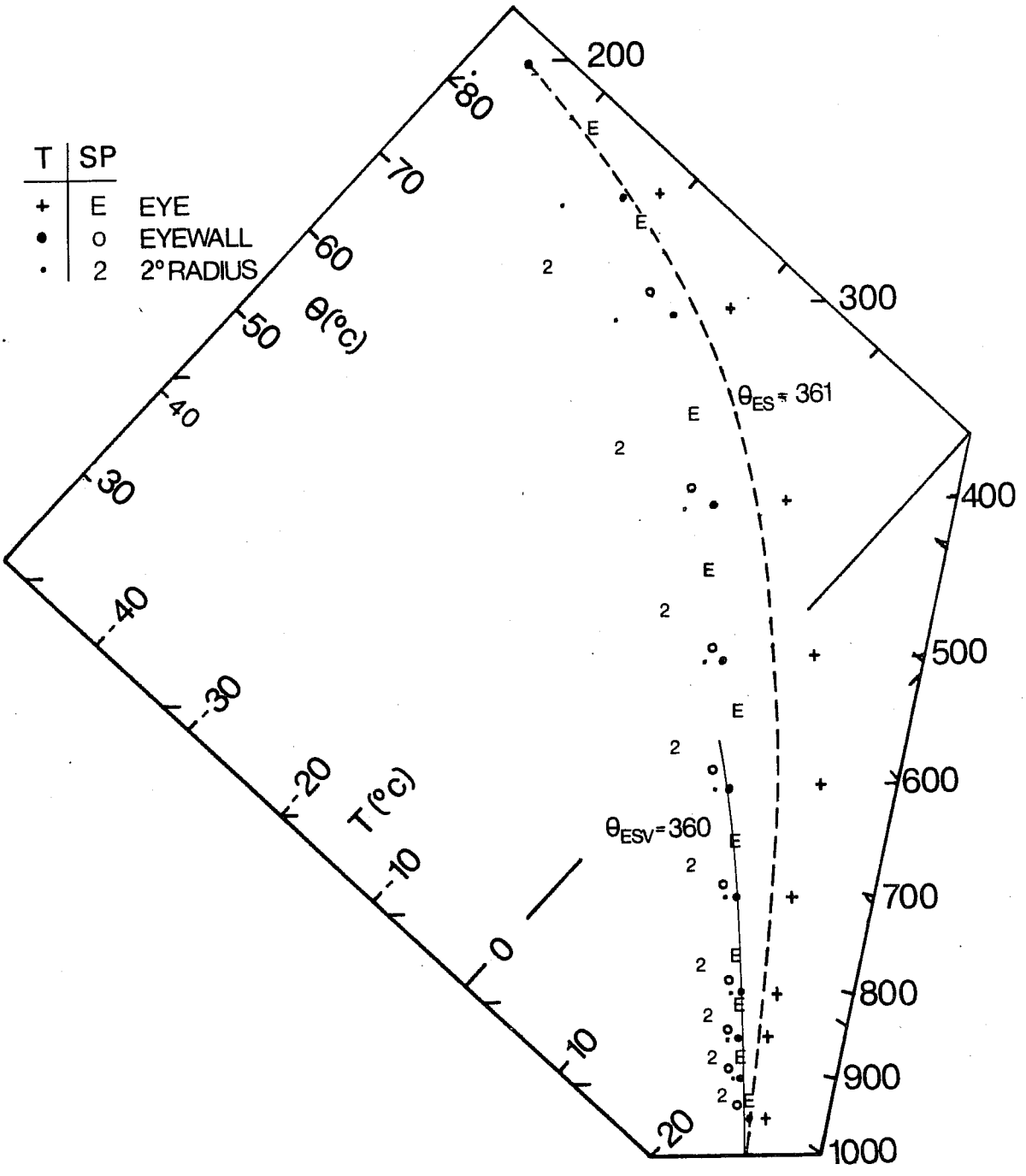


Fig. 1.1 : Composite typhoon sounding inside the eye, the eyewall and 2° radius (Frank, 1977), showing T and SP structure.

The light dots and symbols 2 are the (T, SP) at 2° radius from the storm centre. Here the atmosphere is further from saturation, but has a similar but cooler temperature structure. At 200 mb the eyewall $\theta_{ES}$ ~ 361 K, while at 2° radius $\theta_{ES}$ ~ 357 K, with a corresponding change in $\theta_E$ at the low levels.

Fig. 1.2 shows the deep tropospheric structure for the wake (Barnes and Sieckman, 1984) of GATE (Global Atmospheric Research Program Atlantic Tropical Experiment) convective band composites. These are weaker tropical convective disturbances than the typhoon. They show a very similar profile to Fig. 1.1, with an initial decrease of $\theta_{ES}$ close to a $\theta_{ESV}$ isopleth and then an increase above 600 mb (which is close to the freezing level). The dots and letter F denote the (T, SP) of fast-moving lines (Barnes and Sieckman, 1984) and the cross and letter S denote (T, SP) for slow-moving lines. They show some thermodynamic differences. The $|\mathcal{P}|$ values for each p level are shown (Fast moving on left, slow on right). For reference, $\mathcal{P}$ = -30 mb corresponds to a relative humidity of 85% at 800 mb, 75% at 500 mb and 32% at 200 mb at tropical temperatures. The fast-moving line wake has a drier lower troposphere (as a result of stronger downdrafts). Its 600 mb temperature is cooler, probably as a response to the falling $\theta_E$ in low levels. It is nearly saturated in the upper troposphere corresponding to extensive anvil clouds. The slow-moving line wake shows the reverse, with a moister lower tropospheric structure and $\theta_{ES}$ to 600 mb more closely aligned along a $\theta_{ESV}$ isopleth. It, however, is drier in the upper troposphere. These thermodynamic differences are associated with distinct dynamic features in the wind profile: the fast-moving lines have strong shear between the surface and 650 mb (Barnes and Sieckman, 1984).

2.1.2 Convective equilibrium over land

Figs. 1.3 and 1.4 show examples of average soundings of days of major convective episodes over land (Venezuelan International Meteorological and

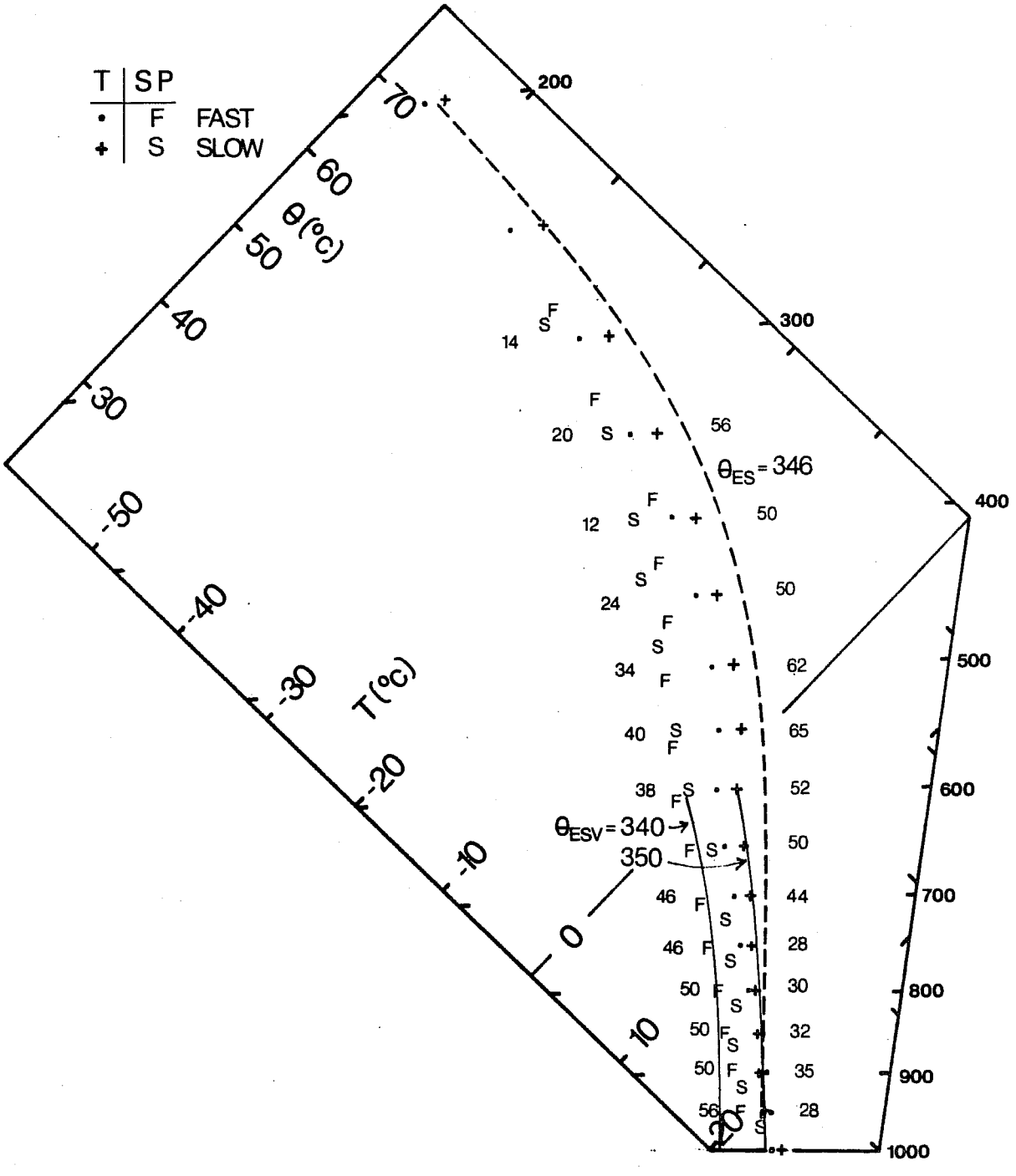


Fig. 1.2 : Composite wake soundings for GATE slow and fast moving lines (Barnes, 1982) showing T, SP and IPI values.

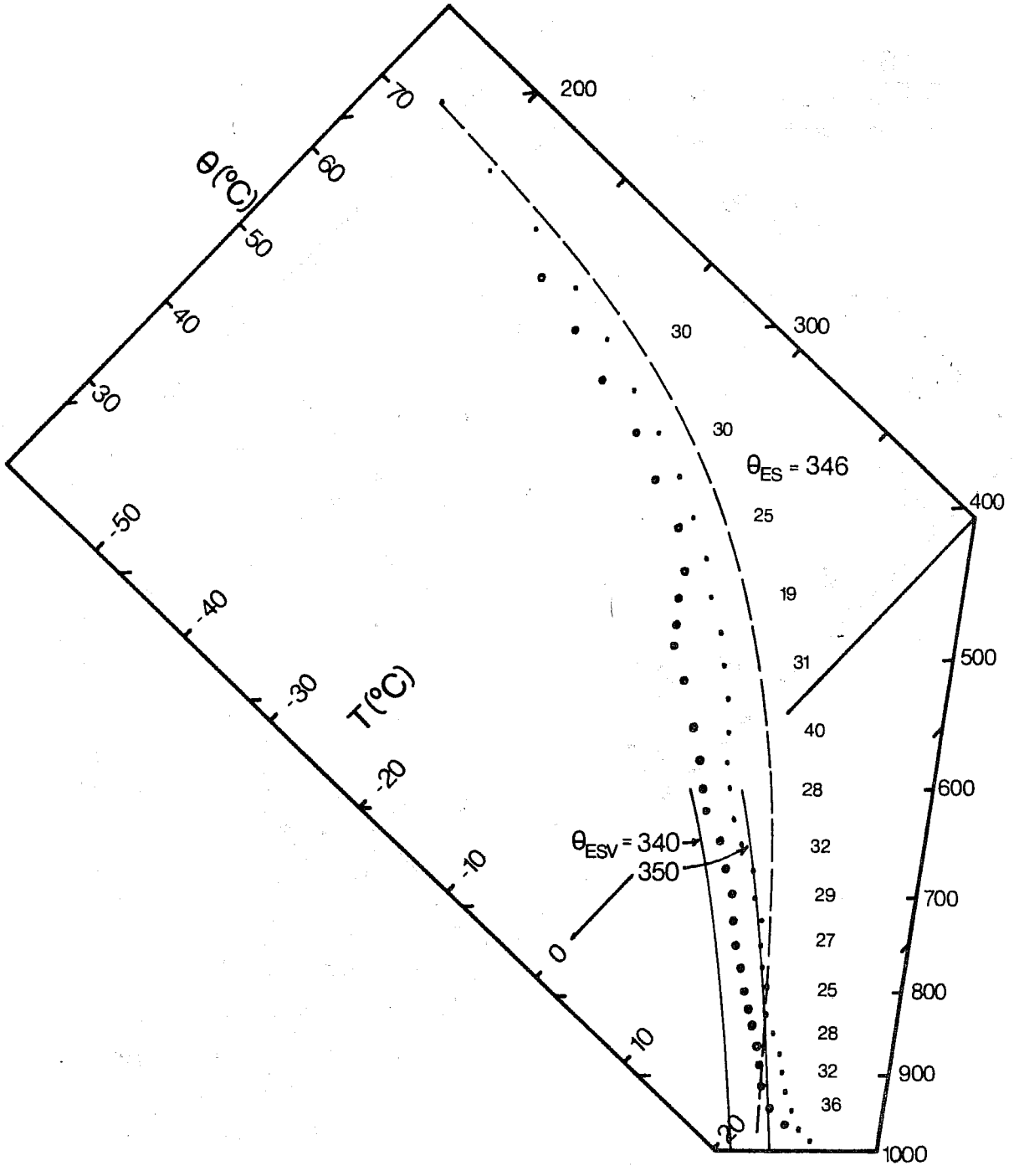


Fig. 1.3 : Composite sounding for 2 September, 1972 showing T and SP structure (6 soundings).

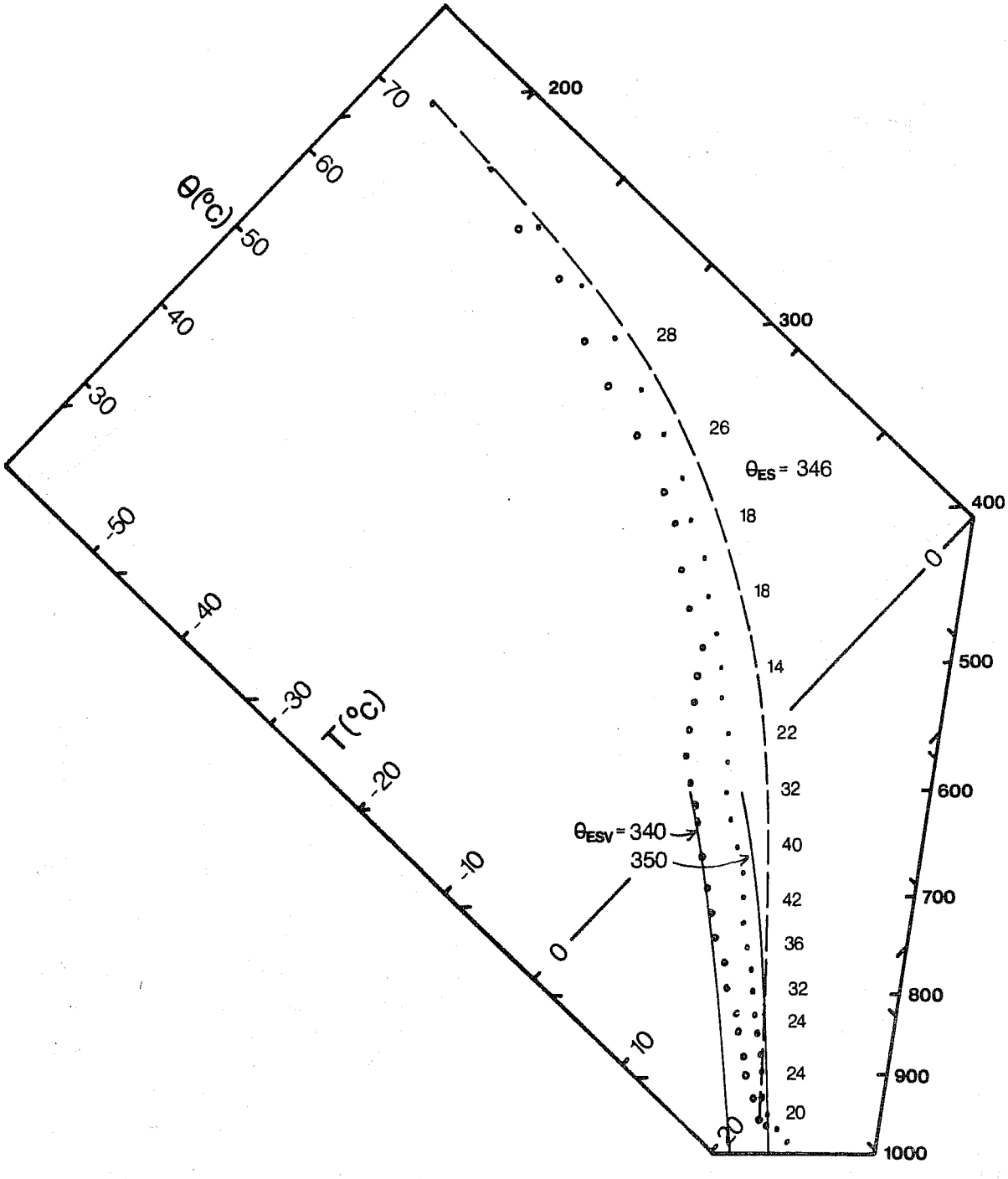


Fig. 1.4 : As Fig. 1.3 for 9 August, 1972 (7 soundings).

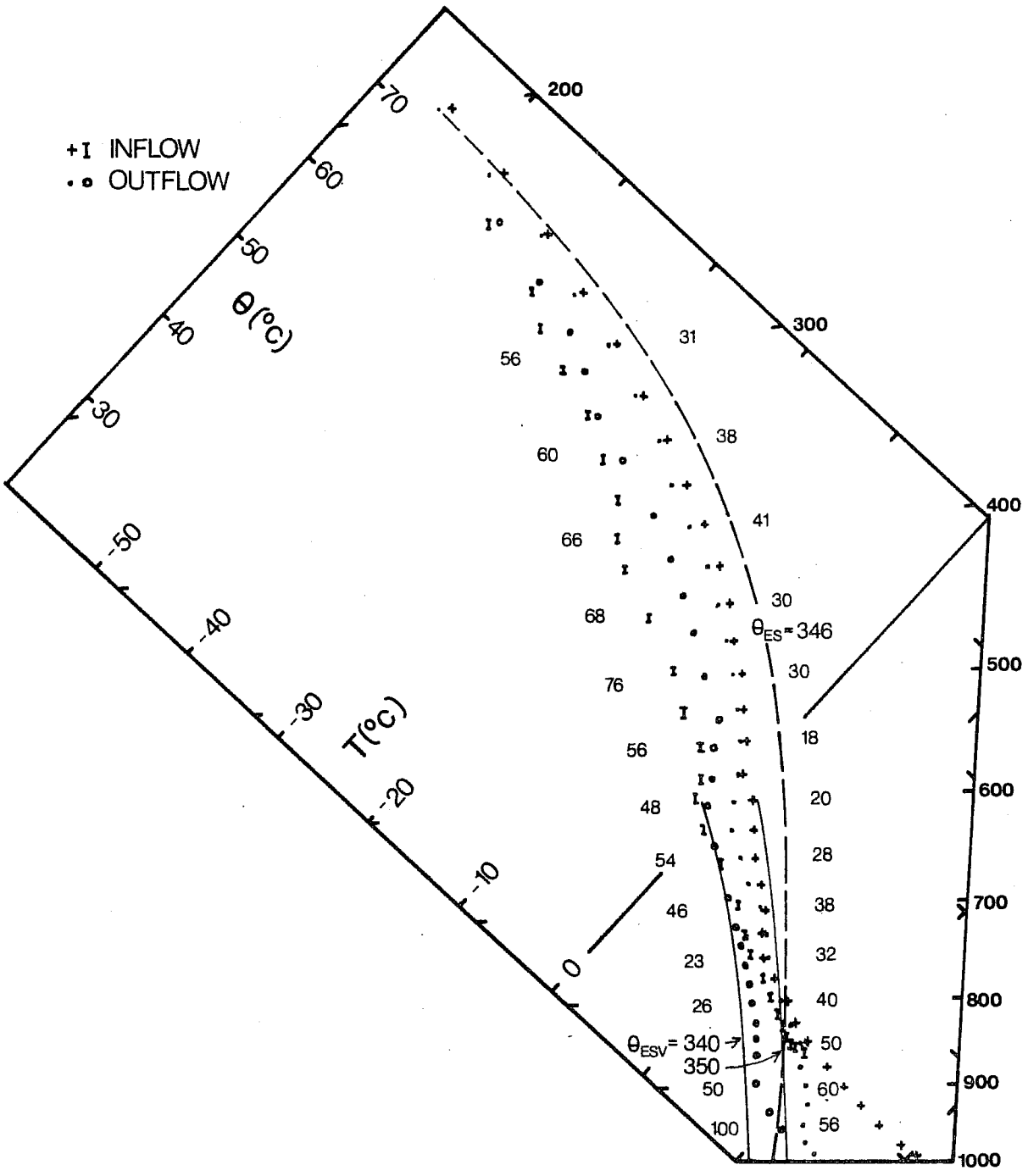


Fig. 1.5 : Profiles of T and SP for inflow and outflow of a Venezuela composite of fast moving storms (Miller and Betts, 1979).

Hydrological Experiment (VIMHEX), 1972). The dots are the temperature structure and the open circles the corresponding SP's. The low-level T structures closely parallel a $\theta_{ESV}$ isopleth to the freezing level (near 600 mb) and then show an increase of $\theta_{ES}$ above. This structure is typical of deep convection in the tropics and may be regarded as more representative of deep convective equilibrium than say a moist adiabatic T structure. These days do not have fast-moving mesosystems.

### 2.1.3 Fast-moving storms over land

Fig. 1.5 shows the inflow and outflow T, SP for a composite of fast-moving storms over Venezuela (Miller and Betts, 1977). Above 600 mb the upper tropospheric temperature structure is similar to Figs. 1.1-1.4. The low-level structure shows a marked drying and cooling of the deep subcloud layer to give values of $\mathcal{P} \approx -50$ mb, very similar to the GATE fast-moving composite, and a low-level outflow SP profile which is close to $\theta_{ESV} \sim 344$ K.

### 2.1.4 Deep convective equilibrium structure: parametric philosophy

Most tropical cumulonimbus have small vertical velocities ($\sim 10 m.s^{-1}$) (Zipser and Lemone, 1980), and must therefore have correspondingly small mean buoyancy excesses (~0.3 K). Traditionally it has been assumed that temperatures on the moist adiabat are representative of parcel buoyancy for unmixed parcels, but this gives estimates for convective available potential energy far in excess of observed vertical kinetic energies. The $\theta_{ESV}$ isopleth which allows for the buoyancy correction for cloud water has a slope ($d\theta/dz$) only 0.9 times that of the moist adiabat: a marked reduction in buoyancy in the low levels (Betts, 1982a). The tendency of deep convective temperature soundings to approach this slope from cloud base to the freezing level

(Figs. 1.1-1.5) suggests that it is $\theta_{ESV}$ rather than $\theta_{ES}$ (the moist adiabat) that is the critical reference process in the low troposphere. In physical terms the atmosphere remains slightly unstable on a $\theta_{ESV}$ isopleth, so that air rising in vigorous cumulus towers remains buoyant until its cloud water is converted to precipitation size particles.

Closer inspection shows that there may be some observable differences between dynamically different convective systems. All (even the nearly saturated hurricane eyewall convection) shows a marked decrease of $\theta_{ES}$ below 600 mb which is the approximate freezing level for this tropical set of data. The temperature structure approximates a $\theta_{ESV}$ isopleth suggesting that the lifting of cloud water is a significant density correction in active convective cells in the first few hundred mb above cloud base. The fast-moving storms show a more unstable $\theta_{ES}$ structure (Figs. 1.2 and 1.5) and correspondingly a drier low-level SP and $\mathcal{P}$ structure associated with stronger unsaturated downdrafts. Perhaps the rapid fall of low-level $\theta_E$ prevents a close approach to mid-level thermal equilibrium (see also below).

Around the freezing level both $\theta_{ES}$ and the SP show a marked stabilization with a steady increase of both in the upper troposphere toward the $\theta_{ES}$ isopleth through a low-level SP. This stable structure is probably associated both with freezing and the fallout of precipitation. Both increase cloud parcel buoyancy and we would expect this increase to be reflected in the mean sounding structure if the convection is not far from buoyancy equilibrium with the environment. This suggests also that the sounding minima in $\theta_{ES}$ just below the freezing level probably reflect not only the buoyancy correction due to the lifting of cloud water in active cells discussed above, but also the melting of falling precipitation.

The actual computation of cloud parcel buoyancy allowing for fallout and partial freezing would require an elaborate cloud model. We shall adopt a different strategy for parametric purposes. If we assume that quasi-equilibrium means that cloud-environment buoyancy differences become small in regions of active deep convection, then the environmental profile will reflect the cloud-scale processes which alter cloud-parcel buoyancy. We can then use the observed thermodynamic structure as the basis for a parametric adjustment procedure. This seems preferable to attempting to generate in a numerical simulation a realistic quasi-equilibrium structure by the use of cloud models (whether simple or complex). To the extent that we can distinguish observationally differences in thermodynamic structure (and cloud fields) for dynamically different types of convection, these could be included in a parametric procedure.

For the parametric model we shall simply constrain $\theta_{ES}$ to have a minimum near the freezing level, by using the $\theta_{ESV}$ isopleth as a reference process in the lower troposphere. A gradient parameter (see Eq.(9)) will be tuned using a GATE wave data set.

The $\mathcal{P}$ structure (related to subsaturation) shows more variability related to important physical processes. Fast-moving storms (Figs. 1.2 and 1.5) with stronger downdrafts have $\mathcal{P} \sim -60$ mb in the low levels (related to a downdraft evaporation pressure scale, Betts 1982b) compared to $\mathcal{P} \sim -30$ mb in the low levels for the GATE slow-moving lines and VIMHEX August 9 and September 2 cases (Figs. 1.2, 1.3 and 1.4). Upper level values of $\mathcal{P}$ are variable in the -20 to -40 mb range: the smaller values (-20) correspond to layers closer to saturation, and presumably to the generation of more extensive cloud layers at outflow levels. For the parametric model, we shall specify the $\mathcal{P}$ structure and use the GATE-wave data set for sensitivity and tuning studies.

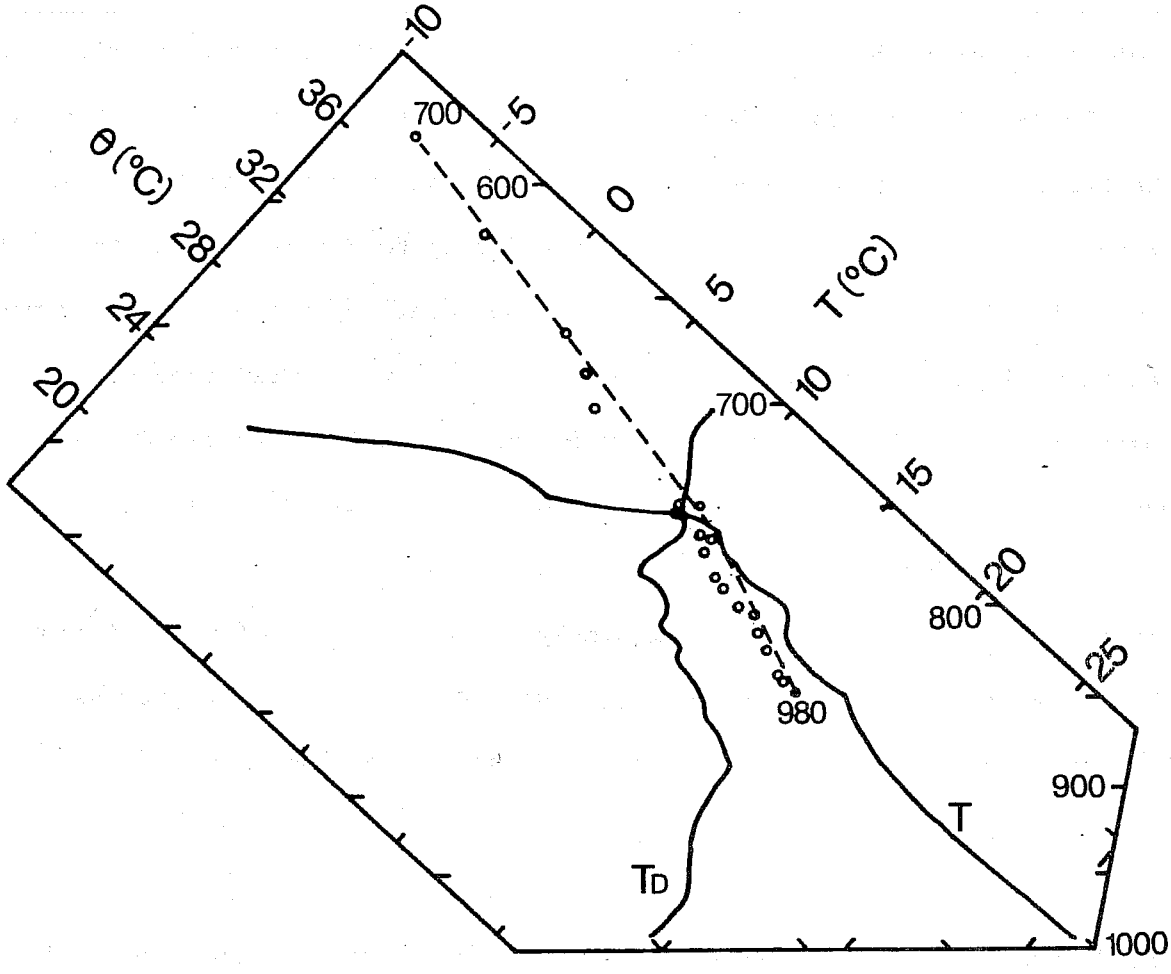


Fig. 1.6 : Late afternoon convective structure, showing SP's lying along a mixing line (Venezuela, 1972).

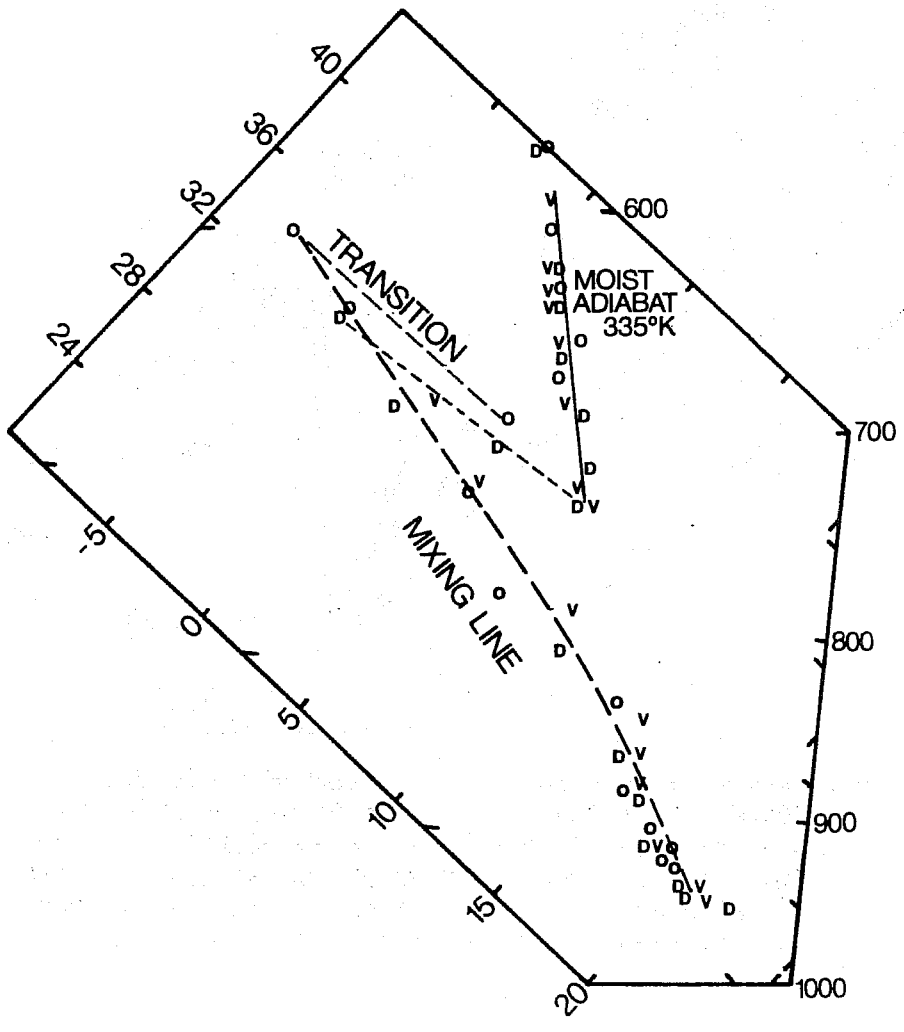


Fig. 1.7 : Soundings at Oceanographer, Vanguard and Dallas on GATE day 258 showing transition between different atmospheric layers.

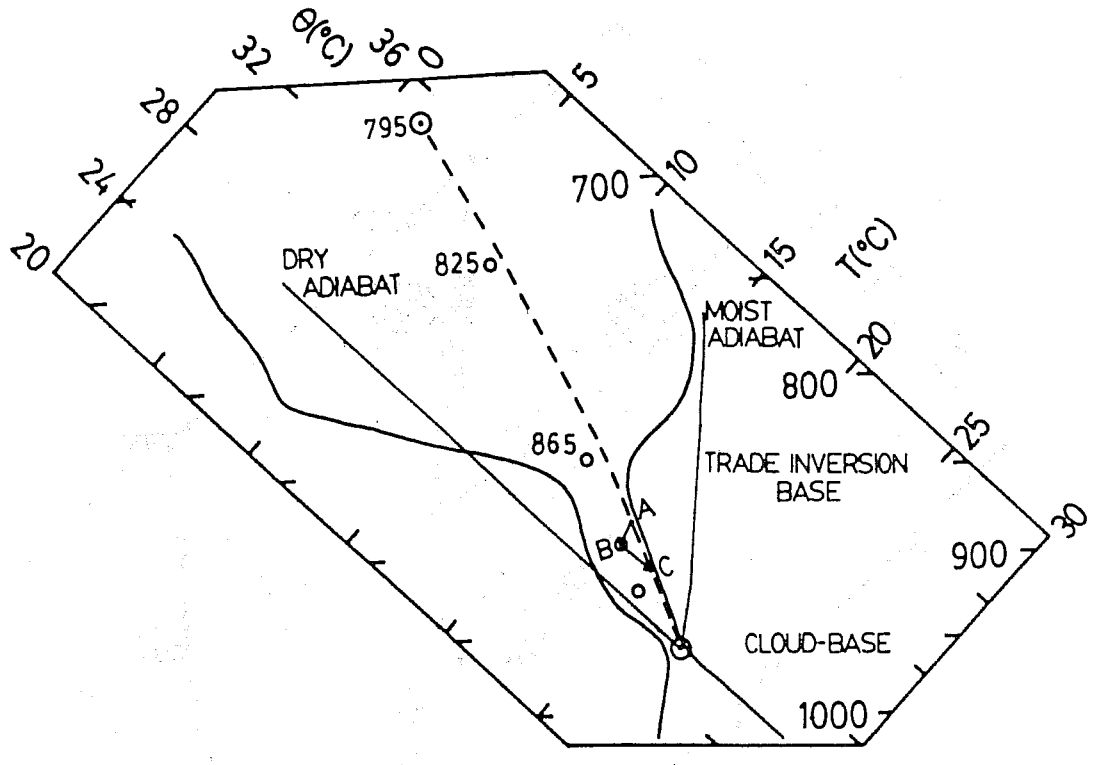


Fig. 1.8 : Three-day sounding for undisturbed trade-wind convection (BOMEX 22-24 June 1969, data kindly supplied by E.M. Rasmusson). Dashed curve is mixing line between inversion top and subcloud air SP's. Open circles are SP's of environment. Arrow AB denotes generation of environmental SP by radiational cooling of air from mixing line.

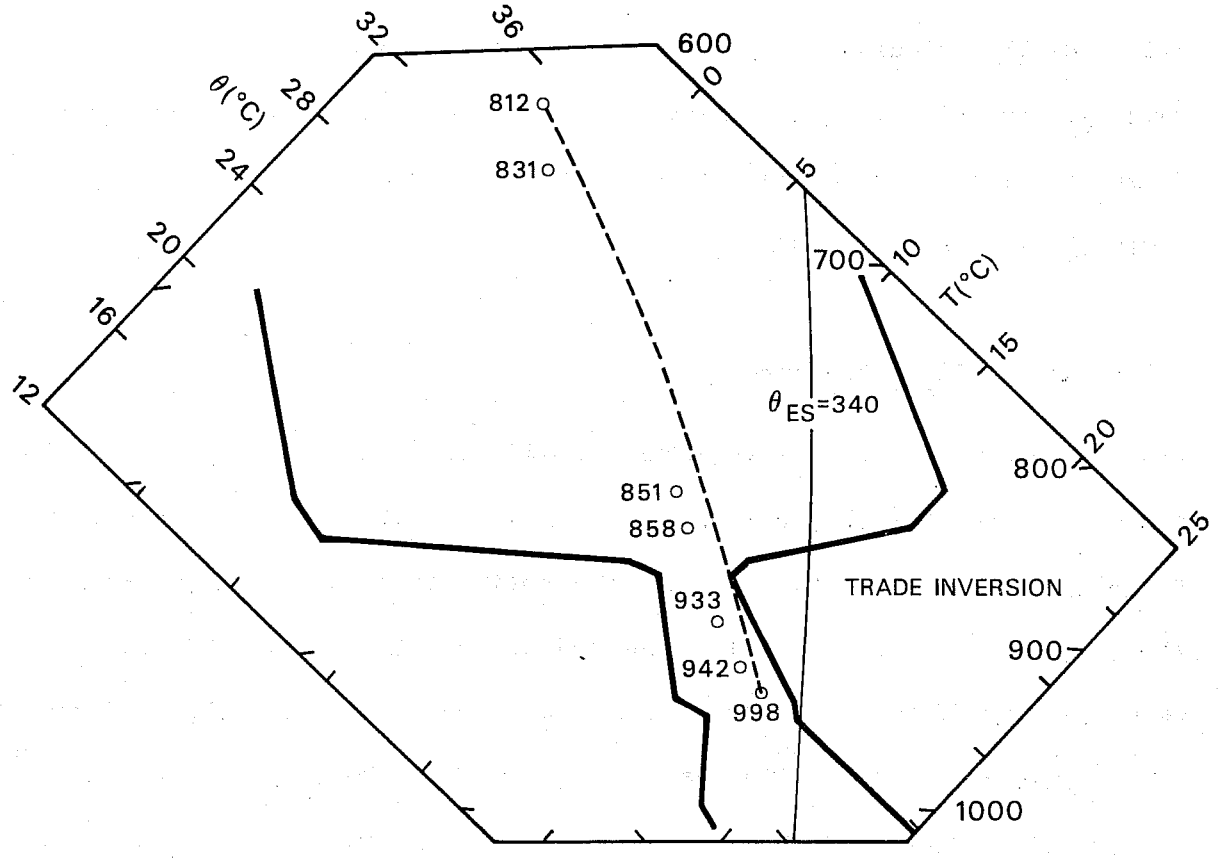


Fig. 1.9 : Undisturbed average sounding (T, $T_d$) for ATEX (7-12 February, 1969). Dashed line is the mixing line between inversion top air and air near the base of the subcloud layer; open circles are environmental SP's.

We adjust from cloud-base to cloud-top. A detailed cloud model is not used to find cloud-top for the parametric scheme. Instead cloud-top is chosen very simply as the parcel equilibrium height found by constructing a moist adiabat through a low-level $\theta_E$.

## 2.2 Shallow cumulus convection: mixing line structure

Cumulus convection is a moist mixing process between the subcloud layer and drier air aloft, and not surprisingly the thermodynamic structure tends toward a mixing line (Betts, 1982a).

### 2.2.1 Mixing line structure

Fig. 1.6 shows the ($T$, $T_D$) structure (solid lines) and corresponding SP's (open circles) from the surface to 700 mb for a late afternoon convective sounding over land in the tropics. The entire SP structure from 980 mb to 700 mb lies close to the mixing line joining the end-points. There is a patch of cloud near 750 mb and a dry layer above, but these large fluctuations of $T$ and $T_D$ only appear as SP fluctuations up and down the mixing line. The temperature structure in the cloud layer below the stable layer at 700 mb is nearly parallel to the mixing line.

In contrast air masses that are not convectively mixed show a distinct discontinuity in the SP structure. An example is given from GATE in Fig. 1.7 in which a nearly moist adiabatic SP structure overlies a convectively mixed layer. Three soundings from nearby ships all show the same air mass transition.

### 2.2.2 Trade cumulus equilibrium

Fig. 1.8 shows a three-day BOMEX average for the undisturbed Trade winds (from Betts, 1982a). The dashed line is the mixing line between cloud-base air and

subsiding air just above the trade inversion. We note that the lapse rate in the conditionally unstable cumulus layer is very close to the mixing curve (as in Fig. 1.6). This suggests that the lapse rate in the lower cumulus layer is controlled by the mixing process. The detailed thermodynamic balance involves radiational cooling as well (Betts, 1982a).

Fig. 1.9 shows an average for an undisturbed period during the Atlantic Trade wind Experiment (ATEX) (Augstein et al, 1973). The structure is similar to Fig. 1.8, although the cloud layer lapse-rate appears slightly more unstable than the mixing line. However, this average was generated by a special procedure, Augstein et al. (1973), designed to sharpen gradients, and may be misleading as a horizontal average.

The shallow convection parameterization scheme, though simplified, is based on these examples and others (not shown).

Cloud-top will be found from the intersection with the sounding of a moist adiabat through a low-level $\theta_E$. The lapse-rate in the cloud-layer below cloud-top will be specified as parallel to that of the mixing line between low level air and air above cloud-top. $\mathcal{P}$ , related to the sub-saturation in the cloud layer, will be specified as independent of height (Figs. 1.6 and 1.8 show sub-saturation roughly constant in the cloud layer). Integral energy constraints then implicitly determines the value of $\mathcal{P}$ . Although the resulting scheme is extremely simple, we shall show that it successfully reproduces the main features of shallow convection.

## 3. CONVECTIVE ADJUSTMENT SCHEME

The scheme is designed to adjust the atmospheric temperature and moisture structure back towards a reference quasi-equilibrium thermodynamic structure in the presence of large-scale radiative and advective processes. Two different reference thermodynamic structures (which are partly specified and partly internally determined) are used for shallow and deep convection.

## 3.1 Formal structure

The large-scale thermodynamic tendency equation can be written in terms of $SP(\underset{\sim}{\bar{S}})$, using the vector notation suggested in Betts (1983), as

$$\frac{\partial \underset{\sim}{\bar{S}}}{\partial t} = - V.\nabla \underset{\sim}{\bar{S}} - \bar{\omega} \frac{\partial \underset{\sim}{\bar{S}}}{\partial p} - g \frac{\partial \underset{\sim}{N}}{\partial p} - g \frac{\partial \underset{\sim}{F}}{\partial p} \qquad (1)$$

where $\underset{\sim}{N}$, $\underset{\sim}{F}$ are the net radiative and convective fluxes (including the precipitation flux). The convective flux divergence is parameterized as

$$- g \frac{\partial \underset{\sim}{F}}{\partial p} = \frac{\underset{\sim}{R} - \underset{\sim}{\bar{S}}}{\tau} \qquad (2)$$

where $\underset{\sim}{R}$ is the reference quasi-equilibrium thermodynamic structure and $\tau$ is an adjustment time representative of the convective or meso-scale processes.

Simplifying the large-scale forcing to the vertical advection, and combining (1) and (2) gives

$$\frac{\partial \underset{\sim}{\bar{S}}}{\partial t} = \bar{\omega} \frac{\partial \underset{\sim}{\bar{S}}}{\partial p} + (\underset{\sim}{R} - \underset{\sim}{\bar{S}})/\tau \qquad (3)$$

Near quasi-equilibrium $\partial \underset{\sim}{\bar{S}}/\partial t \approx 0$ so that

$$(\underset{\sim}{R} - \underset{\sim}{\bar{S}}) \approx \bar{\omega} \frac{\partial \underset{\sim}{\bar{S}}}{\partial p} \tau \qquad (4)$$

We shall find that values of $\tau$ from 1-2 hrs give good results in the presence of realistic forcing. This means that $\underset{\sim}{R} - \underset{\sim}{\bar{S}}$ corresponds to about 1 hour's

forcing by the large-scale fields, including radiation. For deep convection the atmosphere will therefore remain slightly cooler and moister than $\underset{\sim}{R}$. Furthermore, for small $\tau$, the atmosphere will approach $\underset{\sim}{R}$ so that we may substitute $\overline{\underset{\sim}{S}} \approx \underset{\sim}{R}$ in the vertical advection term, giving

$$(\underset{\sim}{R}-S) \approx \omega\tau \frac{\partial \underset{\sim}{R}}{\partial p} \tag{5}$$

from which the convective fluxes can be approximately expressed using (2), as

$$\underset{\sim}{F} = \int \frac{\underset{\sim}{R}-\overline{\underset{\sim}{S}}}{\tau} \frac{dp}{g} \approx \int \left(\overline{\omega} \frac{\partial \underset{\sim}{R}}{\partial p}\right) \frac{dp}{g} \tag{6}$$

(6) shows that the structure of the convective fluxes is closely linked to the structure of the specified reference profile $\underset{\sim}{R}$. By adjusting towards an observationally realistic thermodynamic structure $\underset{\sim}{R}$, we simultaneously constrain the convective fluxes including precipitation to have a structure similar to those derived diagnostically from (1), or its simplified form (6), by the budget method (Yanai et al, 1973; Nitta, 1977).

3.2 Adjustment procedure

We allow the large-scale advective terms, radiation and surface fluxes, to modify the thermodynamic structure $\overline{\underset{\sim}{S}}$. Cloud-top is then found using a moist adiabat through the surface $\theta_E$. Cloud-top height initially distinguishes shallow from deep convection (currently level 11 in the global model; about 760 mb). Different reference profiles are constructed for shallow and deep convection, which satisfy different energy integral constraints. The convective adjustment, $(\underset{\sim}{R}-\overline{\underset{\sim}{S}})/\tau$, is then applied. This implicitly redistributes heat and moisture in the atmosphere as it is adjusted towards $\underset{\sim}{R}$.

The deep convection reference profile $\underset{\sim}{R}_D$ is constructed to satisfy the total enthalpy constraint

$$\int_{p_B}^{p_T} (H_R - H_{\bar{S}}) dp = 0 \tag{7}$$

where $H = C_p T + Lq$ and $p_B$, $p_T$ are a cloud-base level (or low level) and cloud-top pressure respectively. In the tests discussed in Part II, $p_B$ is fixed at $\sigma = 0.96$. The precipitation rate is then given by

$$PR = \int_{p_B}^{p_T} \left(\frac{q_R - \bar{q}}{\tau}\right) \frac{dp}{g} = -\frac{C_p}{L} \int_{p_B}^{p_T} \left(\frac{T_R - \bar{T}}{\tau}\right) \frac{dp}{g} \tag{8}$$

No liquid water is stored in the present scheme.

The adjustment is suppressed if it ever gives $PR < 0$.

For shallow convection the reference profile $\underset{\sim}{R}_S$ is constructed to satisfy the two separate energy constraints

$$\int_{p_B}^{p_T} C_p (T_R - \bar{T}) dp = \int_{p_B}^{p_T} L(q_R - \bar{q}) dp = 0$$

so that the integrated condensation (and precipitation) rates are zero.

### 3.3 Reference thermodynamic profiles

The essence of this convective adjustment scheme is these reference profiles. We initially separate shallow and deep convection by cloud-top.

### 3.3.1 Deep convection reference profile

(a) First guess profile

The temperature profile has a minimum $\theta ES(M)$ at the freezing level, $P_M$. The low level decrease is based on the gradient V of the $\theta_{ESV}$ isopleth multiplied by a weighting coefficient, $\alpha$. The first guess profile is established using (9) and (10). For $p_B > p > p_M$

$$\theta_{ES} = \theta_{ES}(B) + \alpha V \, (p-p_B) \tag{9}$$

where $V = (\partial\theta_{ES}/\partial p)_{\theta ESV}$ ,

For $p_T < p < p_M$

$$\theta_{ES} = \theta_{ES}(M) + (\theta_{ES}(T) - \theta_{ES}(M)) \, (p-p_T)/(p_M-p_T) \tag{10}$$

This is just a linear increase back to the environmental $\theta_{ES}$ at cloud-top, $p_T$. Tests using a GATE-wave data set (see Part II) showed that $\alpha = 1.5$ gave a realistic tropospheric temperature structure. This reference profile in the low troposphere is therefore just slightly unstable to the $\theta_{ESV}$ isopleth, and has a gradient (compared to the dry and moist adiabats) of

$$(\partial\theta_{ES}/\partial p)_R \simeq 0.15 \, (\partial\theta_{ES}/\partial p)_\theta$$

or the equivalent

$$(\partial\theta/\partial p)_R \simeq 0.85 \, (\partial\theta/\partial p)_{\theta ES}$$

The moisture profile is found from the temperature profile by specifying a grid-point mean $\mathcal{P} = p_{s\ell}-p$ at three levels, cloud base ($\mathcal{P}_B$), the freezing level ($\mathcal{P}_M$) and cloud-top ($\mathcal{P}_T$) with linear gradients in between.

For $p_B > p > p_M$, this gives

$$\mathcal{P}(p) = \left[ (p_B-p)\,\mathcal{P}_M+(p-p_M)\,\mathcal{P}_B \right]/(p_B-p_M) \tag{11}$$

and for $p_M > p > p_T$

$$\mathcal{P}(p) = \left[ (p_M-p)\,\mathcal{P}_T+(p-p_T)\,\mathcal{P}_M \right]/(p_M-p_T) \tag{12}$$

In the present scheme $\mathcal{P}_B, \mathcal{P}_M, \mathcal{P}_T$ are chosen negative (unsaturated), with $|\mathcal{P}|$ a maximum at the freezing level.

(b) Energy correction

T(p) and q(p) are computed from $\theta_{ES}(p)$ and $\mathcal{P}(p)$ and then a correction to the reference profile is made to satisfy Eq.(7). We find

$$\Delta H = \frac{1}{(p_B-p_T)} \int_{p_B}^{p_T} (H_R(1)-\bar{H_S})\,dp \tag{13}$$

where $H_R(1)$ is from the first guess reference profile and $\bar{H_S}$ is for the gridpoint thermodynamic structure. A constant correction is applied to the first guess reference profile, at all levels (except the cloud-top level) of

$$\Delta H' = \Delta H\ (p_B-p_T)/(p_B-p_{T'}) \tag{14}$$

where $p_{T'}$ is at the $\sigma$-level below cloud-top. At each level the temperature field is corrected, with $\mathcal{P}$ kept constant, so as to change $H=(C_p T_R+Lq_R)$ by $\Delta H'$. Applying no correction at cloud-top means that the adjustment scheme corrects

the q-field at cloud-top (through the first guess) but not the T-field. This is necessary in the global model to avoid systematic corrections at levels just below the tropopause. However, it is also consistent with cloud-top being near the level of thermal equilibrium. One iteration is made on this energy correction step to ensure the subsequent adjustment conserves energy to high accuracy.

### 3.2.2 Shallow convection reference profile

(a) First guess profile

The slope of the mixing line is computed from the properties of air at the level $p_B$ and the level above cloud-top $p_T+$. This is done by first finding SP on the mixing line corresponding to an equal mixture of air from the levels $p_B$ and $p_T+$. This level, denoted (1), is then used to give a linearized mixing line slope in the lower troposphere using

$$M = (\theta_E(1)-\theta_E(B))/(p_{SL}(1)-p_{SL}(B)) \qquad (15)$$

where $p_{SL}(1), p_{SL}(B)$ are the corresponding saturation level pressures. In the 15 layer gridpoint model we use level 14 for $p_B$ to avoid interaction problems with the diffusion scheme which computes the surface fluxes. The first guess temperature profile is specified as parallel to the mixing line with

$$\theta_{ES}(p) = \theta_{ES}(B) + M(p-p_B) \qquad (16)$$

and constant $\mathcal{P}$ . $\theta_{ES}(p)$ is inverted to give (T,p) which together with $\mathcal{P}$ gives the SP and hence specific humidity.

(b) Enthalpy and moisture correction

Shallow convection is specified as non-precipitating so that the vertical integrals of $C_p T$ and $Lq$ are separately conserved. To ensure this, the first guess T,q are corrected at each level by

$$\Delta T = \frac{1}{(p_B - p_T)} \int_{p_B}^{p_T} T \, dp \tag{17}$$

$$\Delta q = \frac{1}{(p_B - p_T)} \int_{p_B}^{p_T} q \, dp \tag{18}$$

The correction is independent of height so that the slope M of the $\theta_{ES}$ profile, and a $\mathcal{P}$ independent of height are preserved to sufficient accuracy. Constraints (17), (18) mean that the adjustment closely conserves the vertically averaged value of $\mathcal{P}$ through the shallow convective layer.

## 4. CONCLUDING REMARKS

The preceding sections have laid down the observational and theoretical basis of the adjustment scheme. The viability and effectiveness of the scheme, testing and tuning using single-column models, and its incorporation into a global forecast model are described in Part II of this report.

# A NEW CONVECTIVE ADJUSTMENT SCHEME

## PART II: SINGLE COLUMN TESTS USING GATE WAVE, BOMEX, ATEX, AND ARCTIC AIRMASS DATA SETS

by

A. K. Betts and M. J. Miller

CONTENTS PAGE

1. INTRODUCTION 28

2. DEEP CONVECTION 29

2.1 GATE-wave data set 29

2.2 Optimum parameter set 29

2.3 Sensitivity tests 38
2.3.1 Changing adjustment time-scale $\tau$ 38
2.3.2 Changing instability parameter $\alpha$ 39
2.3.3 Changing saturation pressure departure 39

2.4 Interactive surface fluxes 47

3. SHALLOW CONVECTION 48

3.1 BOMEX data set 48

3.2 ATEX data set 53

4. ARCTIC AIRMASS TRANSFORMATION 57

5. CONCLUDING REMARKS 62

## 1. INTRODUCTION

The convective parameterisation scheme introduced in Part I was tested and tuned using a series of single column data sets. A GATE-wave data set (derived from Thompson et al, 1979) was used to test and develop the deep convection scheme. BOMEX (from Holland and Rasmusson, 1973) and ATEX (from Augstein et al, 1973 and Wagner, 1975) data sets were used to test and develop the shallow convection scheme. A fourth data set for an Arctic air-mass transformation (from Økland, 1976) was used to test both schemes with strong surface fluxes.

## 2. DEEP CONVECTION

### 2.1 GATE-wave data set

The grid-point model is run as a single column model with prescribed GATE phase III radiation (from Cox and Griffith, 1979) and prescribed heat and moisture tendencies due to adiabatic processes (from Thompson et al, 1979). The adiabatic forcing terms have a wave structure with 80 hr period. The model is integrated in time from an initial sounding using the convection scheme. The temperature and moisture structure, the precipitation and the vertical profile of the convective heating and drying terms as a function of time can be compared with those diagnosed from observations. Most of the sensitivity tests will be done with surface fluxes prescribed as well (from Thompson et al, 1979), using an 18-level single column version of the Centre's model. (The cloud-base level was specified as the lowest model level (about 982 mb). Section 2.4 will show results with an extra level below cloud-layer and an interactive boundary layer scheme.

### 2.2 Optimum parameter set

We shall present first an optimum parameter set (Table 2.1) to show how well the scheme can reproduce the structure of the mean GATE-wave. Section 2.3 shows how these parameters were selected using sensitivity tests.

| Adjustment time Eq.(2) (hrs) | Stability parameter Eq.(9) | Subsaturation parameters Eqs.(11)(12) cloud-base freezing level cloud-top | | |
|---|---|---|---|---|
| | | $\mathcal{P}_B$ | $\mathcal{P}_M$ | $\mathcal{P}_T$ (mb) |
| 2 | 1.5 | -25 | -50 | -38 |

Table 2.1 Convection scheme optimum parameters

Fig. 2.1a,b shows the 80 hrs mean vertical structure of the moisture and heat budgets. The upper figure shows the prescribed moisture advection and the convective response, and the lower figure the prescribed adiabatic forcing term, the convective heating and the model 'physics' (convective scheme, plus prescribed radiation and surface fluxes). The mean balance is very precise, although the lower troposphere cools and the upper troposphere warms slightly. Figs. 2.2a,b show temperature and dewpoint for the computed 40 hrs and 80 hrs sounding compared with the observations showing the same result. At 40 hrs (the wave trough) the agreement between model scheme and the observed mean structure is very good, although the convection scheme does not reproduce the subsequent drying out of the upper troposphere at the ridge (80 hrs). Figs. 2.3, 2.4, 2.5 compare the time-height cross-sections for the data (observed structure and diagnosed convective source terms) with those predicted by the model using the convection scheme.

Fig. 2.3 shows the evolution of the wave in equivalent potential temperature for a) observations and b) model prediction using the convection scheme. The agreement is good, although as in Fig. 2.2, the data is warmer and moister at the lowest level. Fig. 2.4 shows the same comparison for relative humidity showing fairly good agreement. The convection scheme does not maintain relative humidity well at 200 mb near cloud-top. Fig. 2.5 and 2.6 compare

diagnosed and computed convective heat source and moisture sink (plus surface fluxes), showing how well the parameterisation scheme reproduces the general wave structure of the convective source terms with their maximum at different pressure levels. The agreement is excellent.

Fig. 2.7 compares the observed rainfall and that computed by the model. We see good agreement in amplitude but not in phase. The convection scheme which is closely coupled to the moisture advection, cannot reproduce the observed lag of the precipitation which appears to be due to subgrid-scale storage of moisture presumably in the cloudfields (Betts, 1978; Frank, 1979).

In general the parameterisation scheme does well in reproducing the structure of the convective source terms and the precipitation. In its present form it does not reproduce subgrid-scale moisture storage. The deficiencies in the low level structure seen in Fig. 2.2 can be markedly reduced using an improved resolution and an interactive surface boundary layer (see Section 2.4). Some deficiencies near cloud-top are always likely because the adjustments at this level are always sensitive to the exact specification of cloud-top height in terms of the limited model vertical resolution. Further tuning may be possible. The GATE tests were first run with a cloud-top interpolated between model levels in the specification of the adjustment profile Eq.(10). However, this proved to be an unnecessary complication and was dropped from the scheme for the subsequent interactive (Section 2.4) boundary layer test and global model tests. In these sections, 2.2 and 2.3, we have retained the interpolated cloud-top because a few of the results, although substantially the same, are smoother (cloud-top does not jump between levels) and are therefore easier to compare.

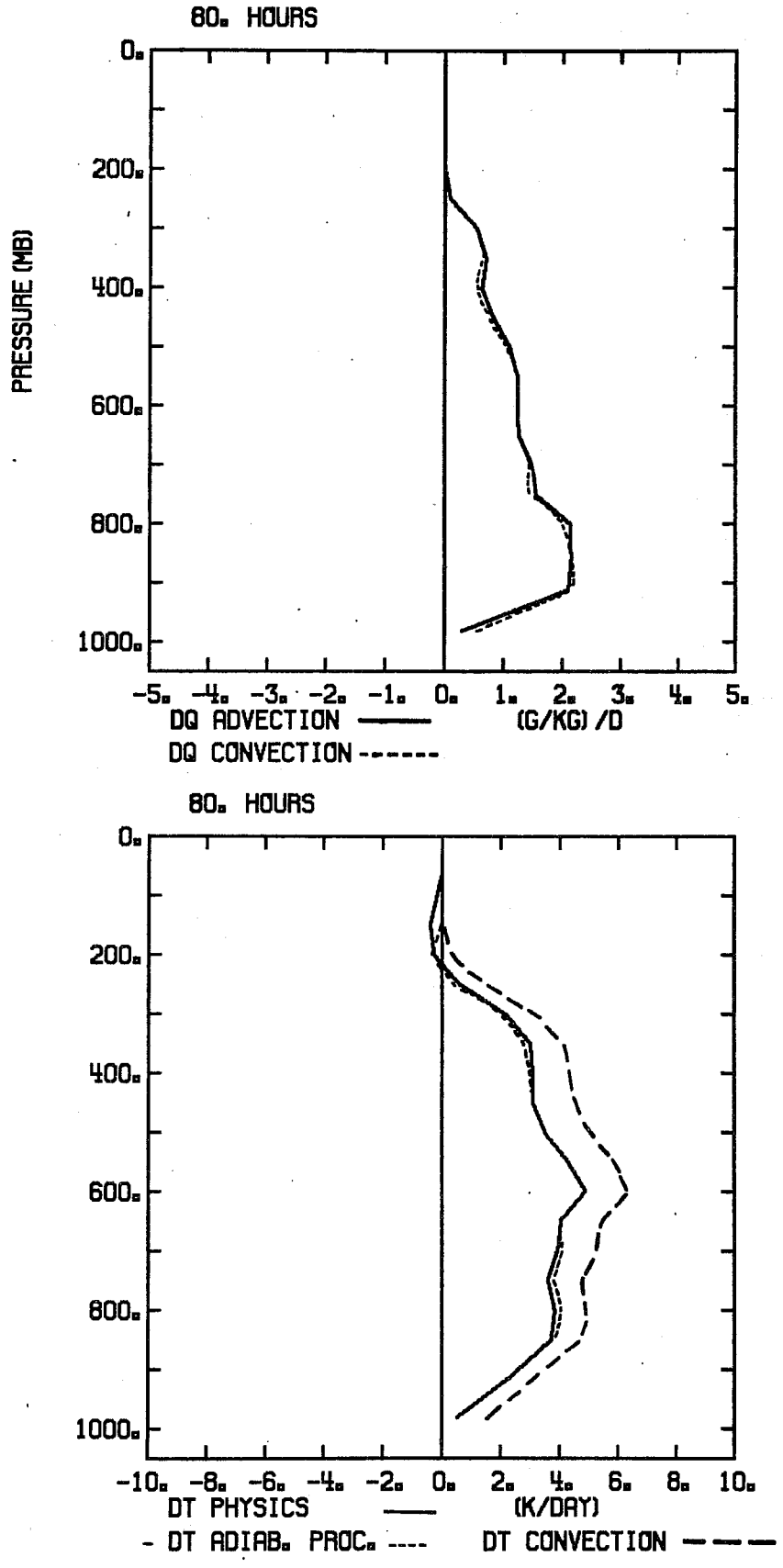


Fig. 2.1 80 hr mean vertical structure of prescribed adiabatic forcing terms and parameterised drying and heating for GATE-wave data due to convection and surface fluxes.

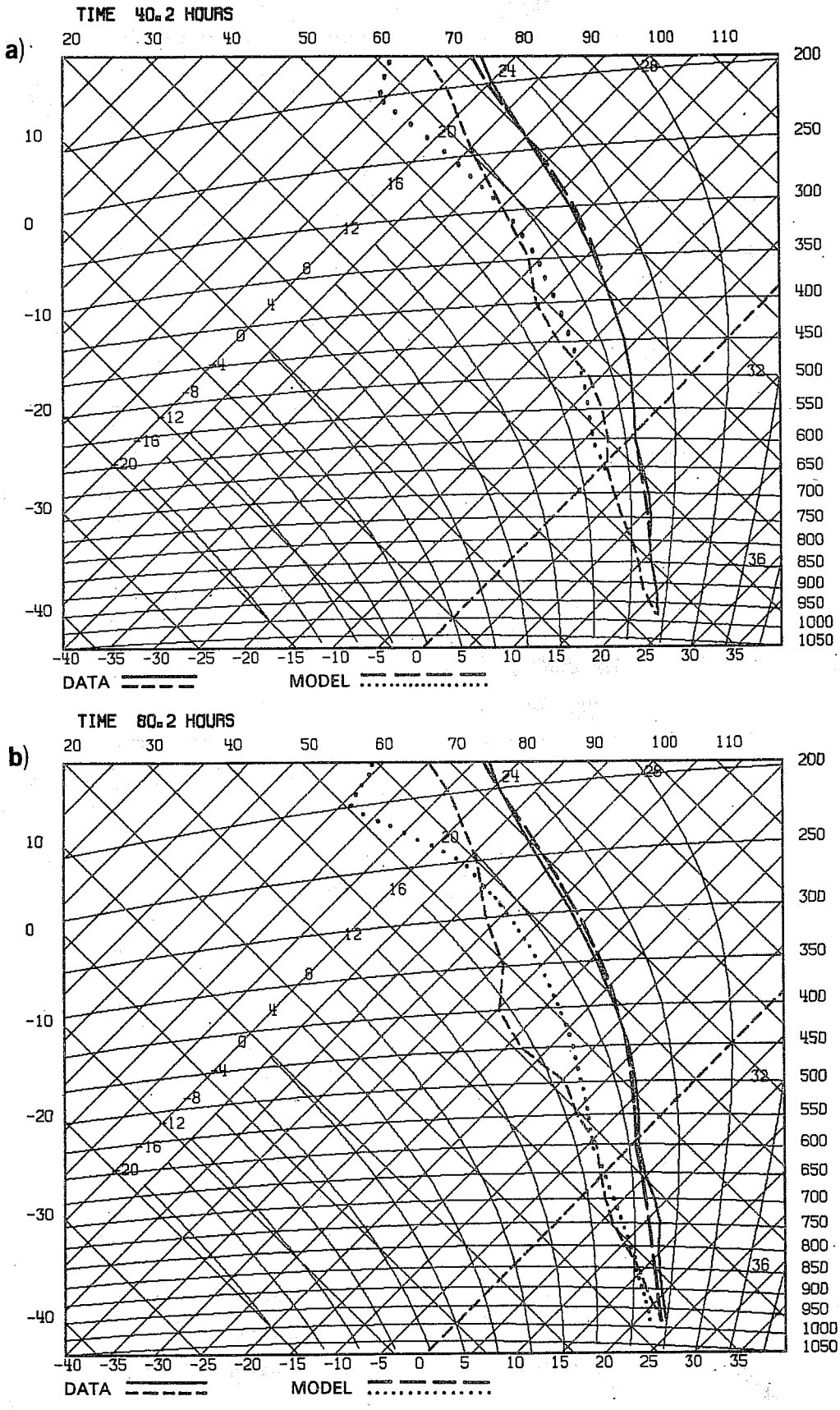


Fig. 2,2 Comparison of observed sounding (T, $T_D$) and computed sounding a) 40 hours (trough) and b) 80 hours (ridge).

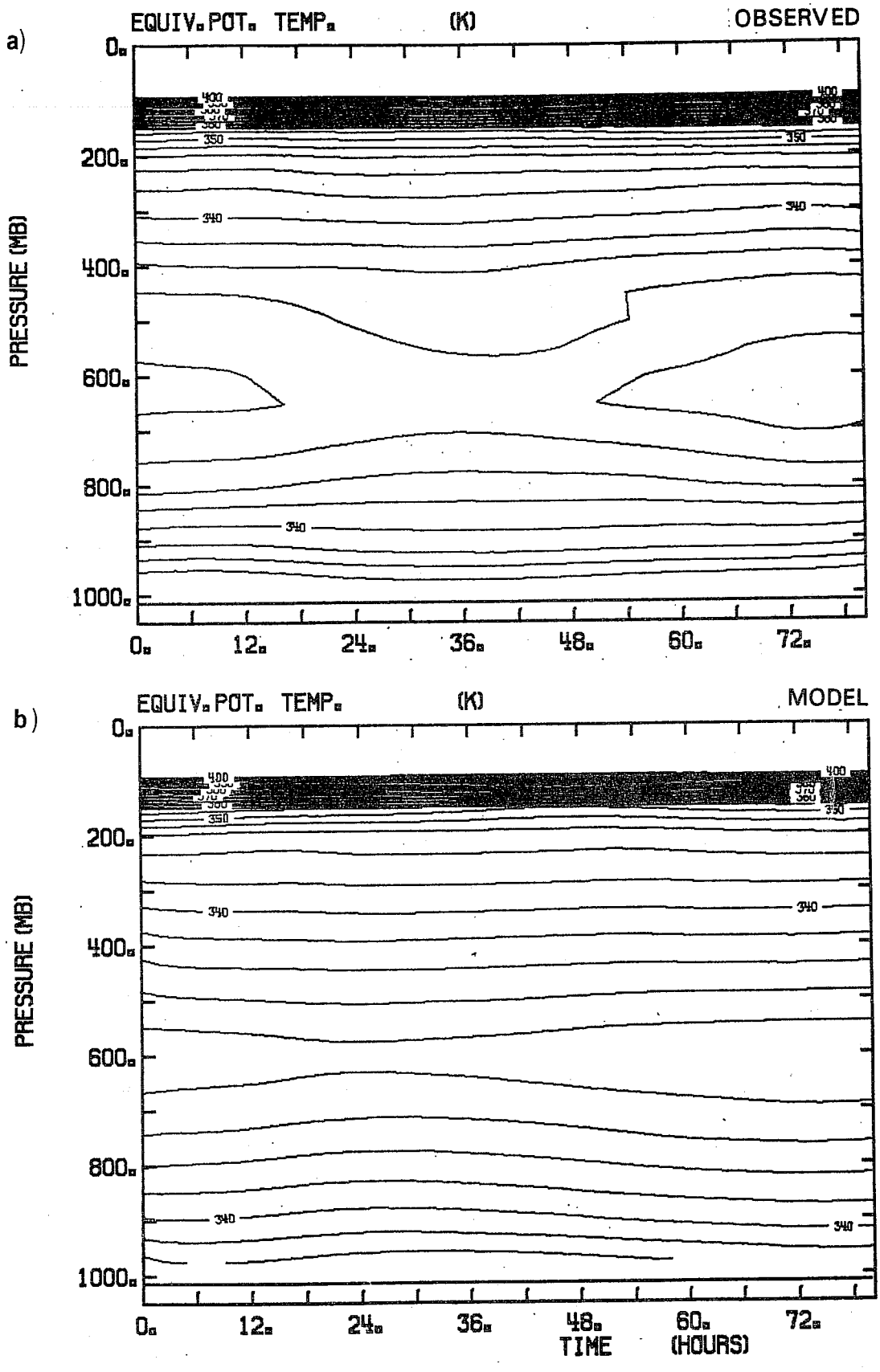


Fig. 2.3 Comparison of a) observed and b) computed $\theta_E$ structure of GATE-wave.

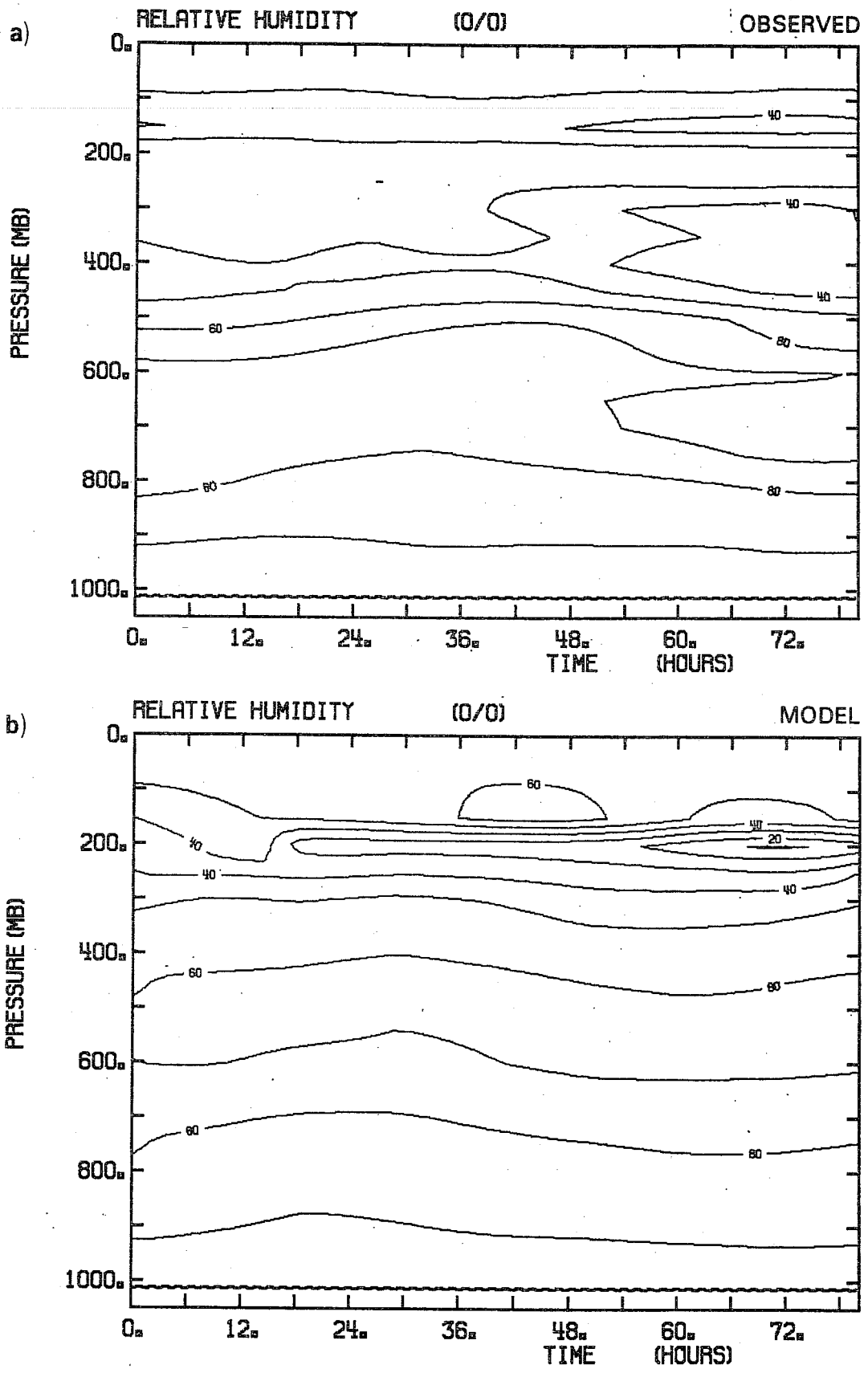


Fig. 2.4 Comparison of a) observed and b) computed relative humidity for GATE-wave.

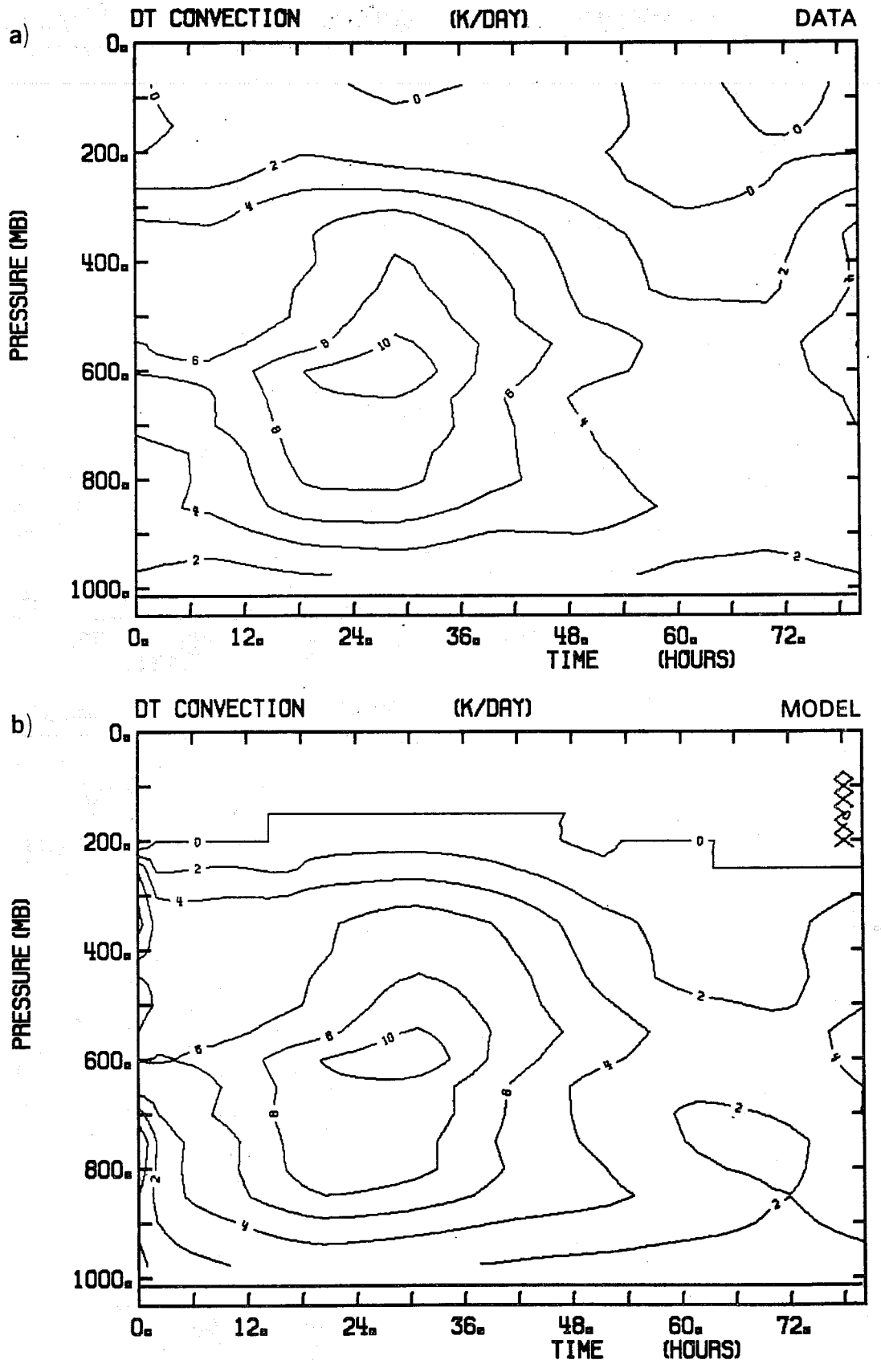


Fig. 2.5 Comparison of a) diagnosed and b) computed convective heating for GATE-wave data.

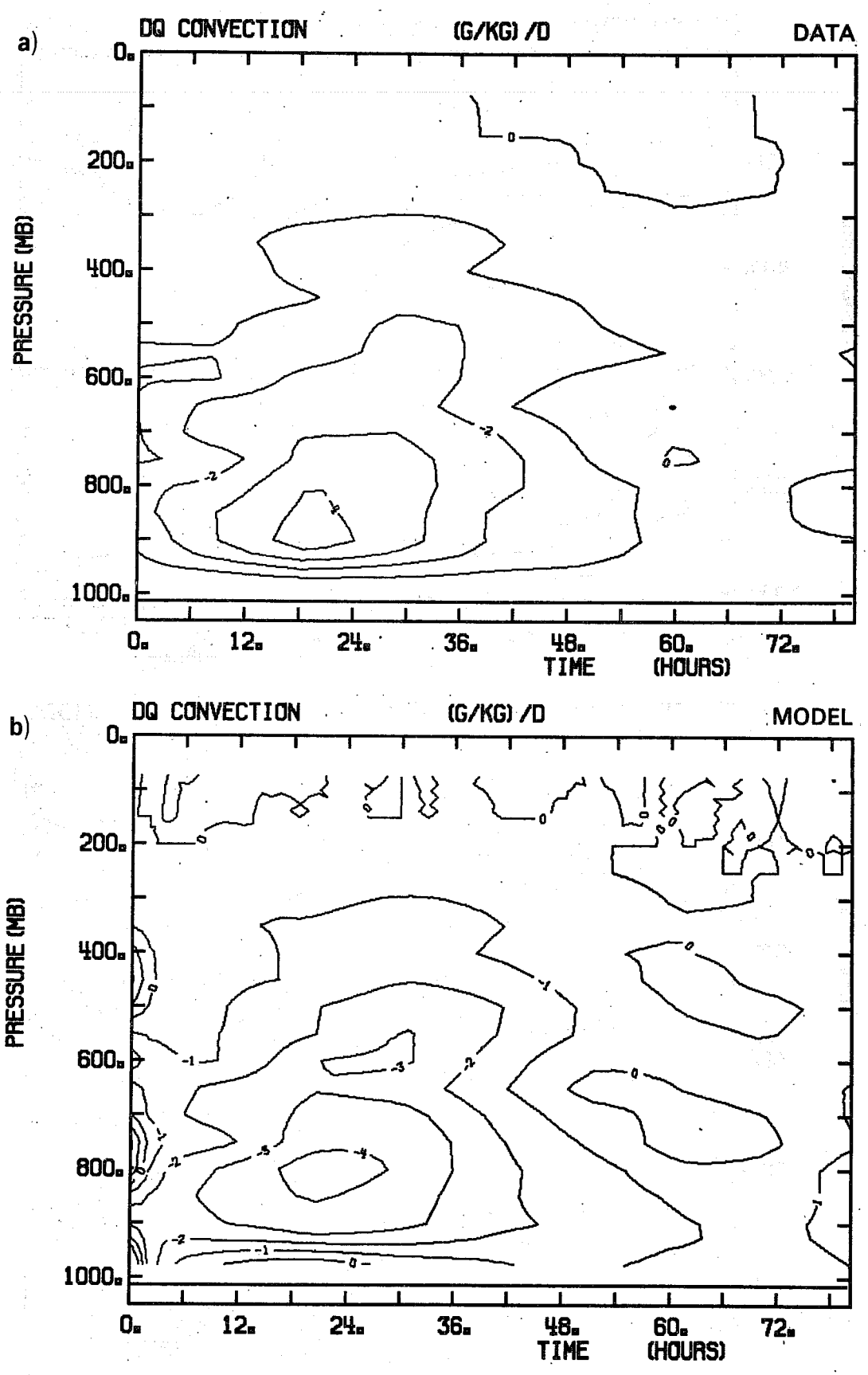


Fig. 2.6 As Fig. 2.5 for convective drying.

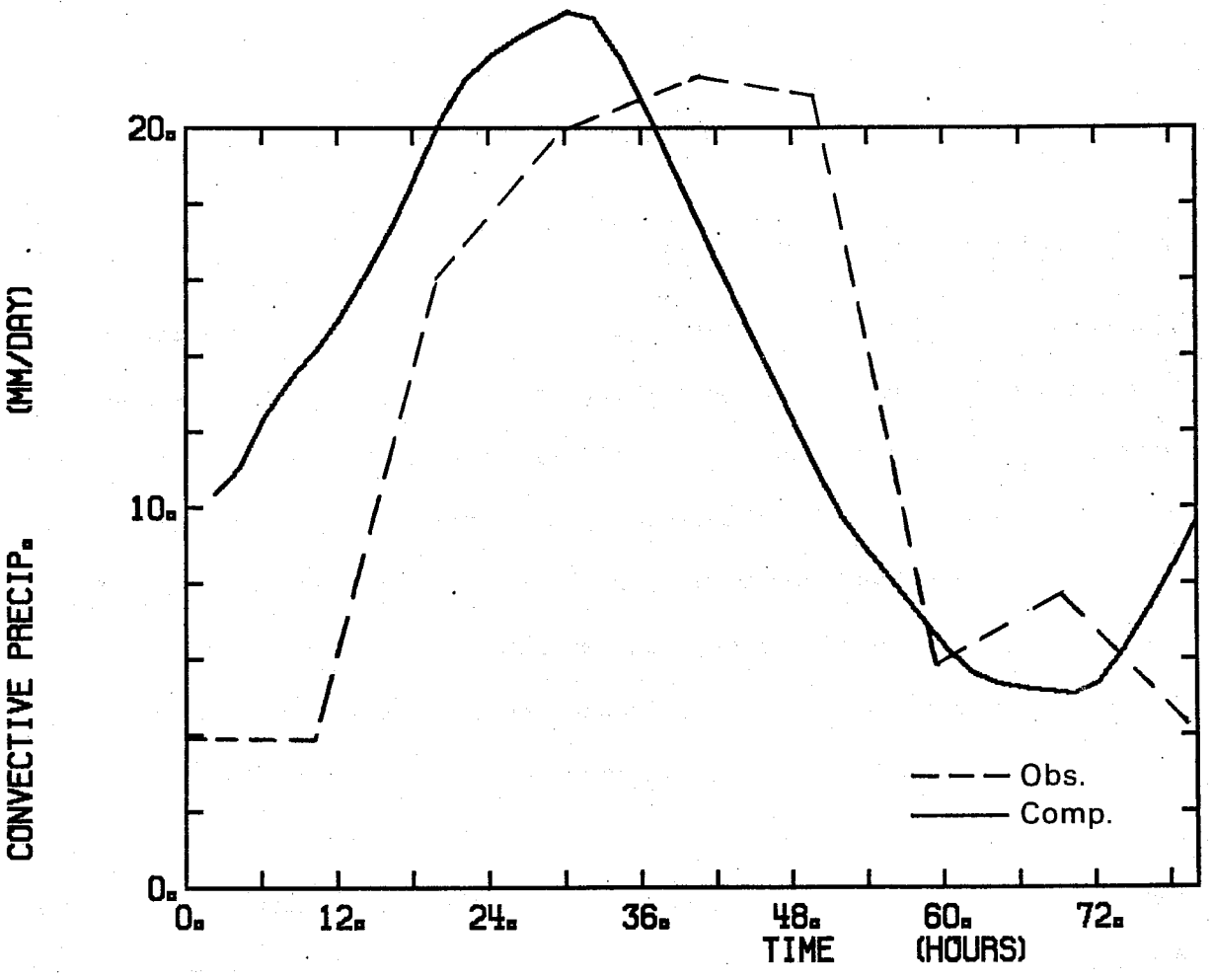


Fig. 2.7 Comparison of observed and computed rainfall.

## 2.3 Sensitivity tests

The parameters used in 2.2 were selected after running a series of sensitivity tests. One of the advantages of this adjustment scheme is that its parameters are readily tuned separately by comparison with an observational data set. Our basic parameters will be $\tau$ = 2 hrs, $\mathcal{P}$ = -30 mb (independent of height) and $\alpha$ = 1.0. Each will be varied separately, while keeping the others constant.

### 2.3.1 Changing adjustment time-scale $\tau$

The adjustment time-scale determines the lag of the convective response to large-scale forcing. With small $\tau$ the model adjusts rapidly towards the specified thermodynamic profile, while with larger $\tau$, the model amosphere moves in the direction of the large-scale forcing. Fig. 2.8 shows the wave in relative humidity (RH) for $\tau$ = 1, 2, 3, 5 hrs ( $\mathcal{P}$ = -30 mb, $\alpha$ = 1.0). For small $\tau$, the wave nearly disappears, while for any larger $\tau$ (>5 hrs), the atmosphere saturates in the wave trough where the large-scale forcing is large. $\tau \sim 2$ hrs gives a wave amplitude in RH similar to that observed (see Fig.2.4). Some parameters such as the overall precipitation and the vertical temperature structure are affected rather little by changing $\tau$. The phase of the precipitation is shifted (Fig. 2.9) as $\tau$ increases, but even for $\tau$ = 5 hrs (which gives an unrealistic wave in the relative humidity) the model precipitation is ahead of that observed. As mentioned in Section 2.2, this is because the adjustment scheme does not allow for subgrid-scale storage of water, which appears to be responsible for the lag of precipitation behind moisture convergence in the GATE data (Betts, 1978; Frank, 1978).

### 2.3.2 Changing instability parameter $\alpha$

The parameter $\alpha$ (Eq.9) determines the slope of the temperature profile in relation to the $\theta_{ESV}$ isopleth, and hence the mid-tropospheric $\theta_{ES}$ minimum. This slope is easy to compare with observational data. Fig. 2.10 shows the comparison of the $\theta_{ES}$ structure for the data, $\alpha = 1.5$ (which is a good fit) $\alpha = 0.0$ (almost a moist adiabat) and $\alpha = 3.0$ (which is very unstable in the low troposphere.

### 2.3.3 Changing saturation pressure departure $\mathcal{P}$

$\mathcal{P}$ is closely related to subsaturation, so changing $\mathcal{P}$ alters the equilibrium relative humidity. It does not change the $\theta_E$ structure significantly, so that the lower troposphere becomes warmer and dries as $\mathcal{P}$ increases. The changes in the upper troposphere are much smaller. Figs.2.11a,b shows the sounding structure at 80 hrs for $\mathcal{P} = -20$ and -40 illustrating this. For = -10 mb the atmosphere saturates during the wave pasage. Fig. 2.12 shows the computed precipitation for $\mathcal{P} = -20, -30, -40$ mb. After the initial adjustment phase the precipitation is almost independent of $\mathcal{P}$ . In the initial adjustment phase, smaller values of $\mathcal{P}$ mean an adjustment towards a moister atmosphere. This initially reduces precipitation for small $\mathcal{P}$ . Indeed for faster adjustment times ($\tau$ = 2 hrs is shown), the computed "precipitation" may initially be negative (Fig. 2.12). These negative values can easily be suppressed by delaying the convective adjustment until the atmosphere has been sufficiently moistened by the large-scale forcing that the precipitation is positive. (This is done in the global model). Suppressing "negative precipitation" has no affect on the subsequent integration after a few hours. For $\mathcal{P}$ = -40 mb, the convection scheme is initially intermittent

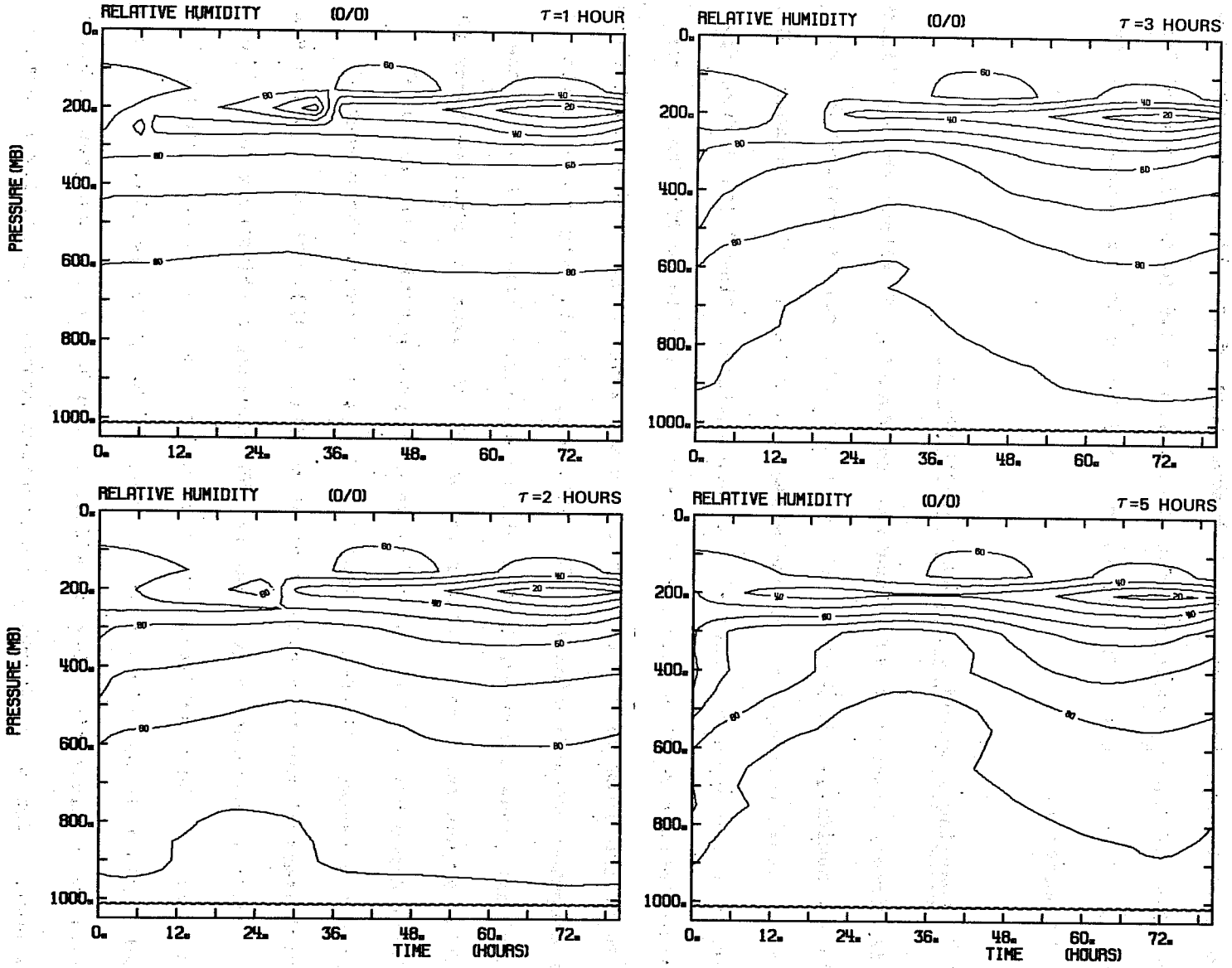


Fig. 2.8 Relative humidity wave for adjustment time-scales, τ=1, 2, 3, 5 hours.

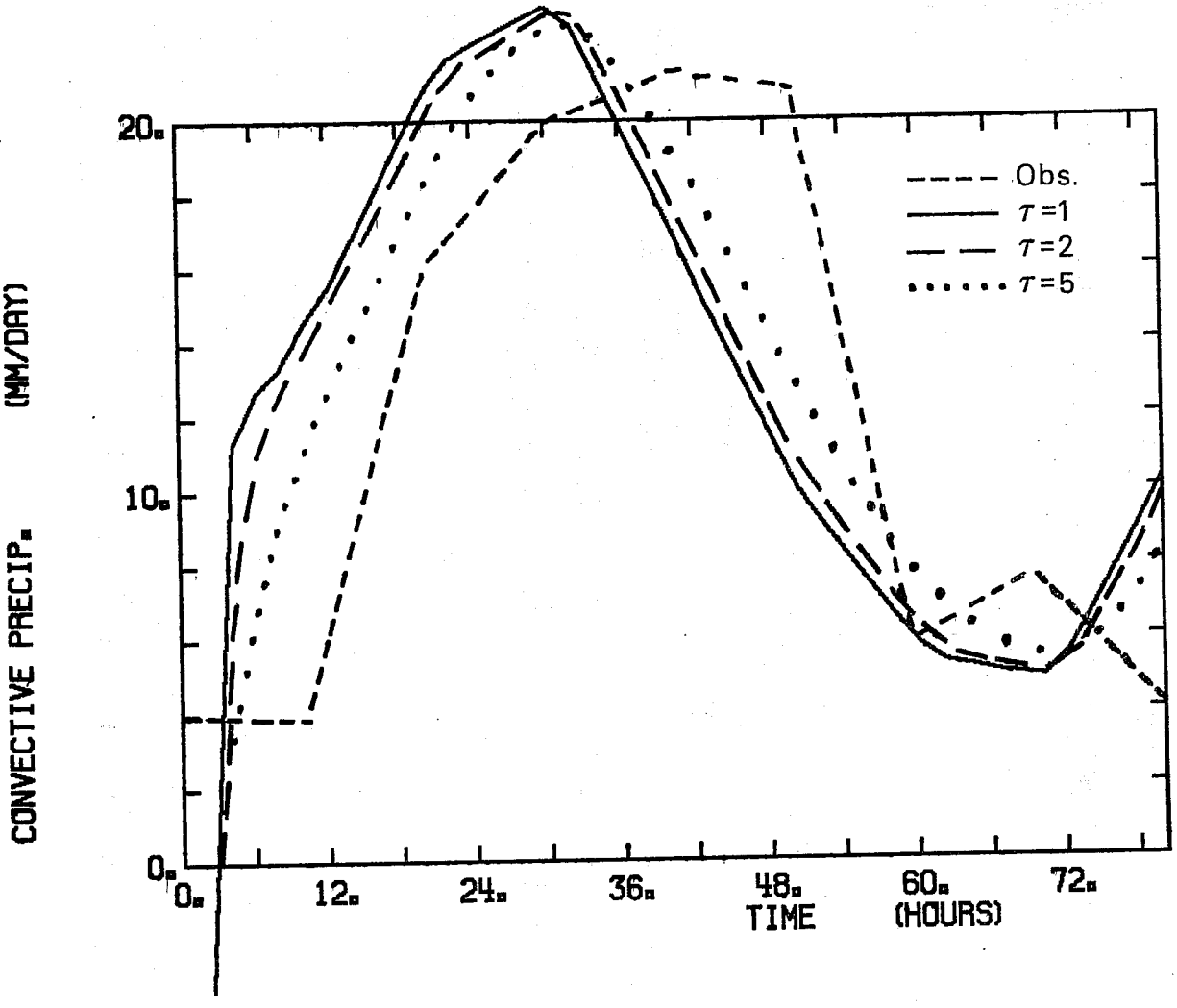


Fig. 2.9 Precipitation curves for τ=1, 2 and 5 hours compared with observed precipitation.

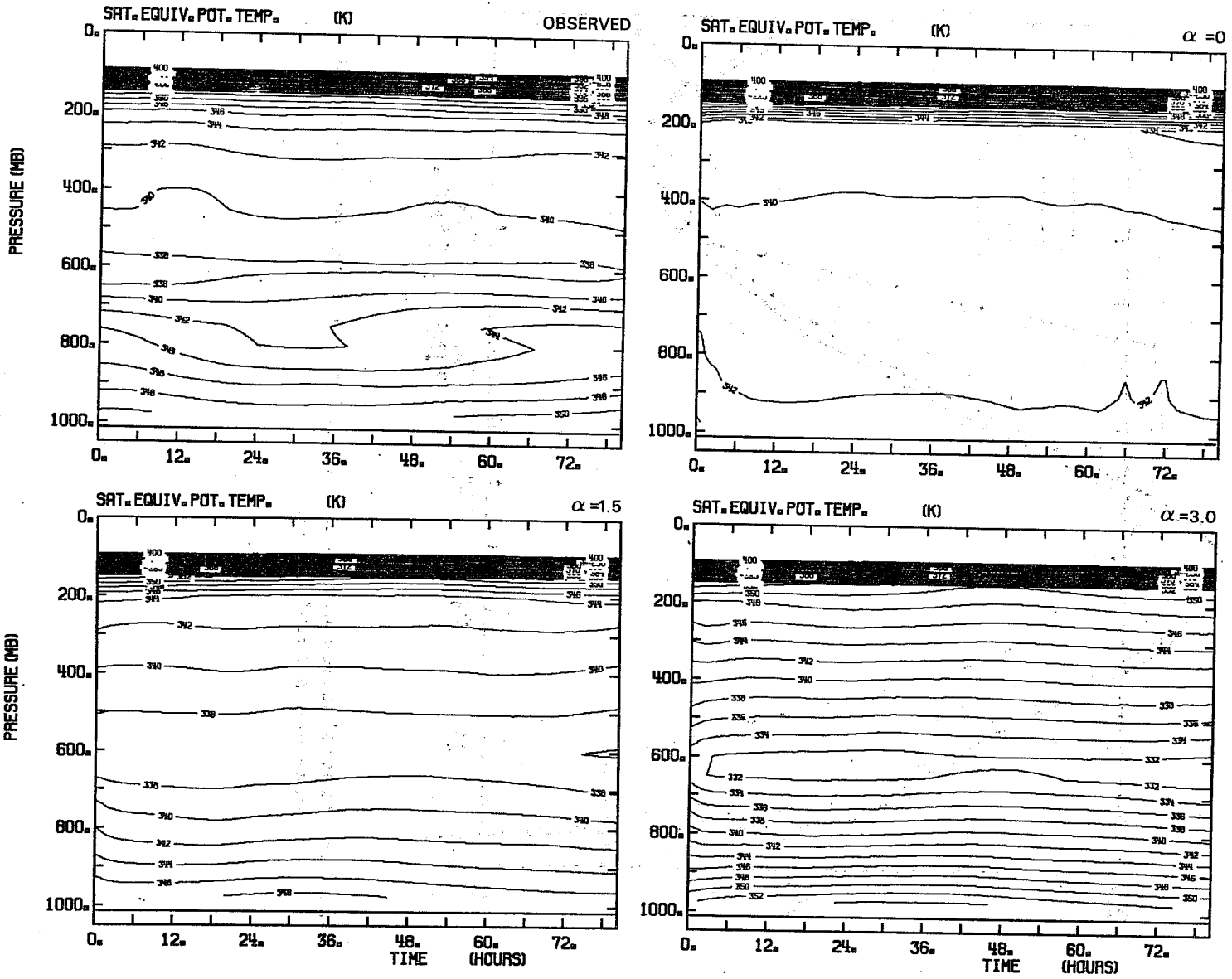


Fig. 2.10 Comparison of observed $\theta_{ES}$ structure of wave with model structure for stability parameter $\alpha$=1.5, 0, and 3.

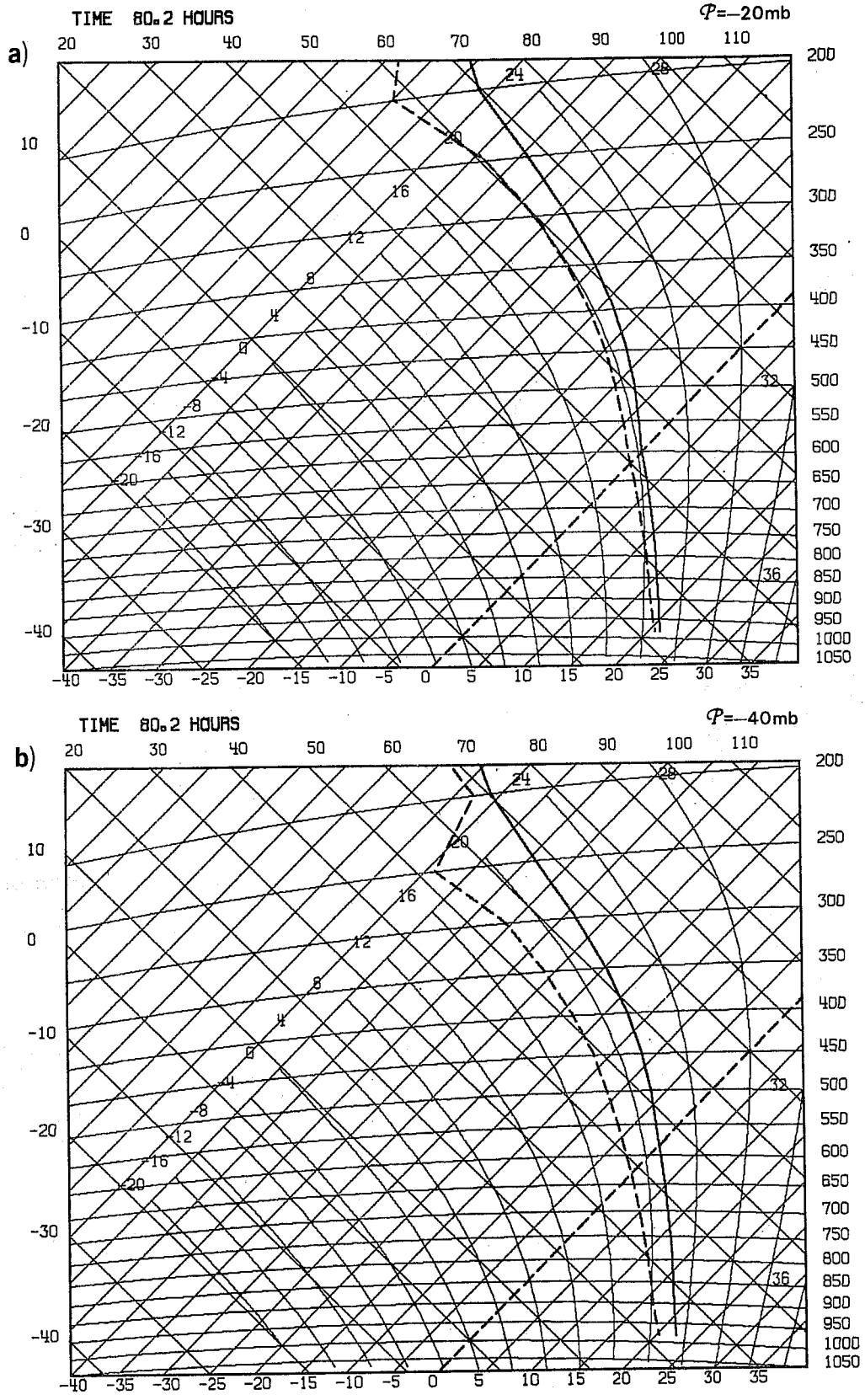


Fig. 2.11 Model thermodynamic structure at 80 hrs for subsaturation parameter a) $\mathcal{P}$ =-20 mb and b) $\mathcal{P}$ =-40 mb ($\alpha$=1, $\tau$=2 hrs).

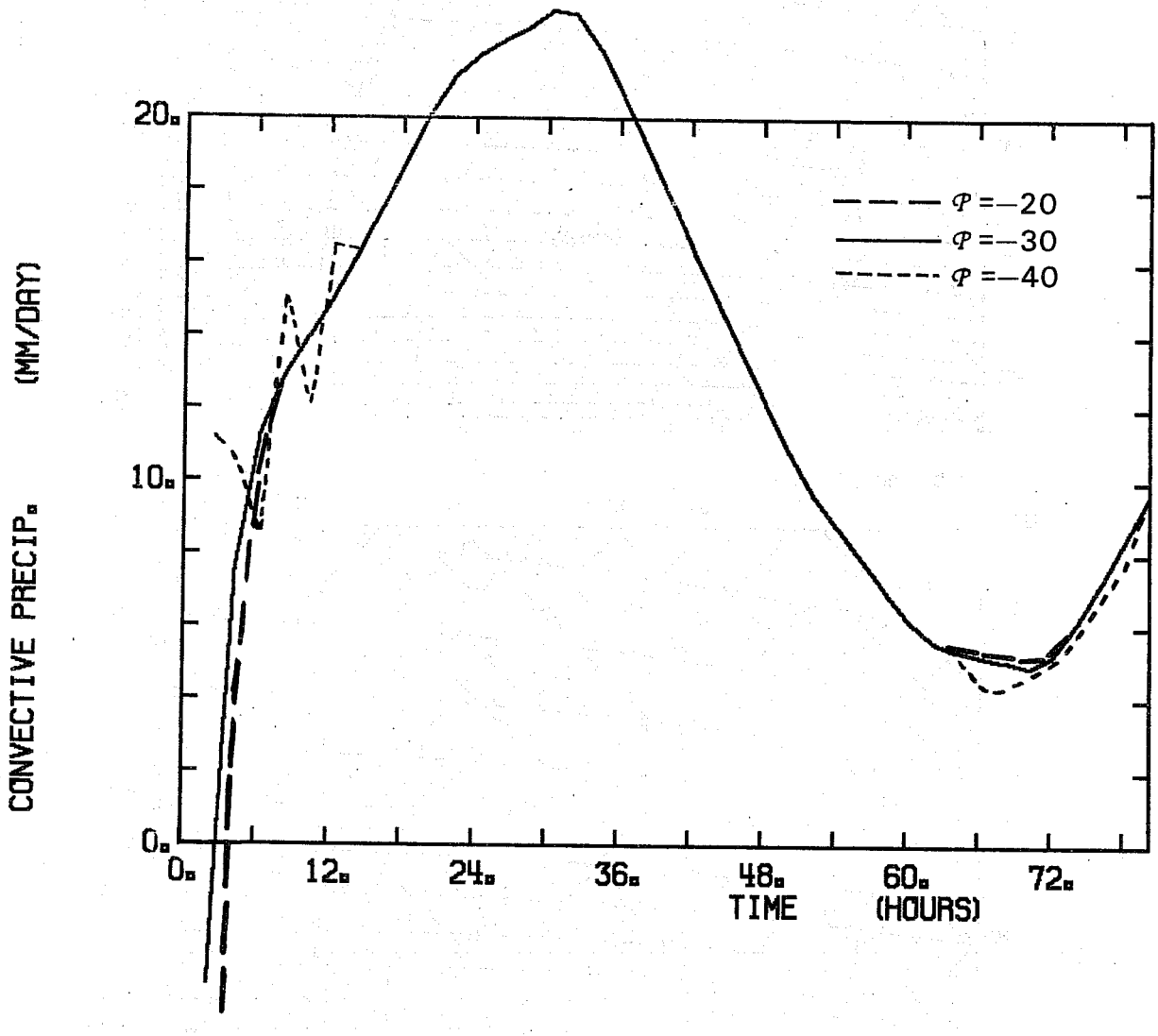


Fig. 2.12 Model precipitation for $\mathcal{P}$ =-20, -30 and -40 mb with $\alpha$=1.0 and $\tau$=2 hours.

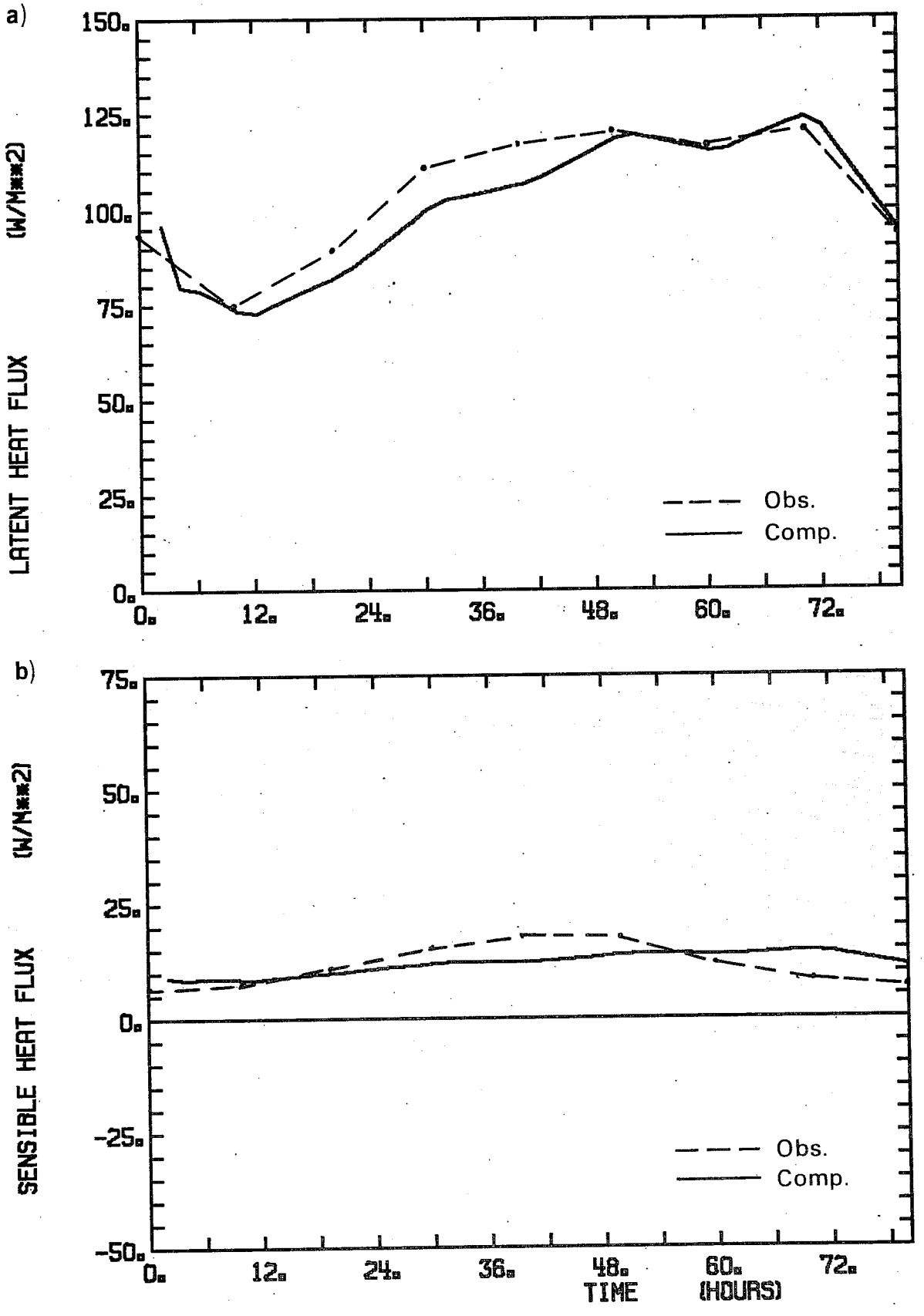


Fig. 2.13 Comparison of observed (dashed) and computed surface fluxes (solid line) with an interactive boundary layer for GATE-wave. Comparison of observed and computed fluxes of a) latent heat and b) sensible heat with an interactive boundary layer for GATE-wave.

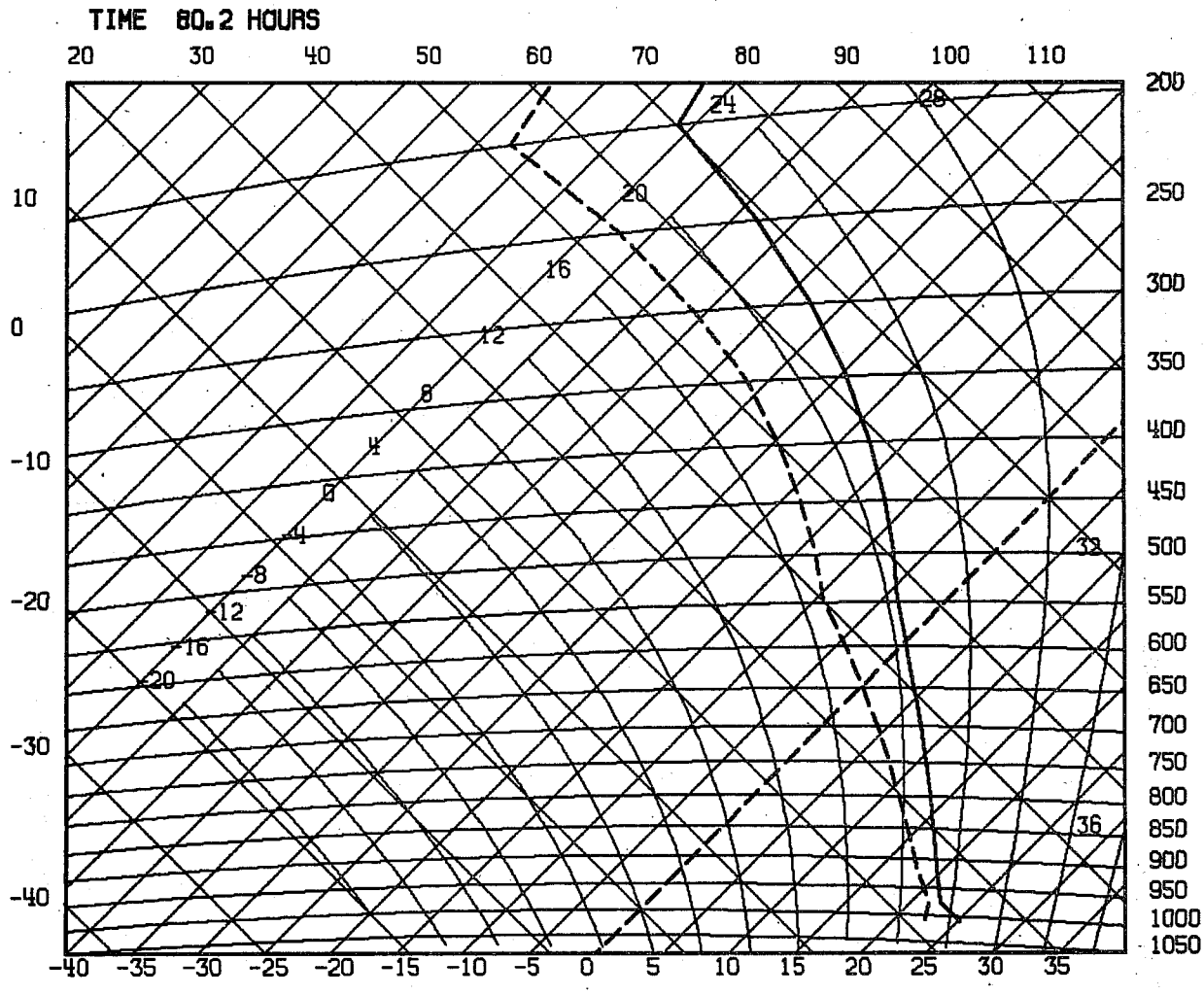


Fig. 2.14 GATE model structure at 80 hours with interactive boundary layer.

(Fig. 2.12) as the cloud-top selection scheme (which uses a moist adiabat through a low level $\theta_E$) sees negative buoyancy in the low levels until $\theta_E$ is increased sufficiently by the surface fluxes. This intermittancy does not affect the time-averaged behaviour of the scheme.

The profile of $\mathcal{P}$ , given in Table 2.1, was chosen to give the best overall fit to the vertical structure of relative humidity in the wave (2.4).

## 2.4 Interactive surface fluxes

The tests in Sections 2.2 and 2.3 were run with specified surface fluxes added to the lowest model layer (about 982 mb). A version of the model with an extra layer near the surface (and the layer at 150 mb removed) was run with an interactive boundary layer diffusion scheme to compute the surface fluxes. This requires, in addition, the sea surface temperature (fixed at 27°C) and the surface wind-speed. Thompson et al (1979) used mean surface winds and a bulk drag coefficient ($C_E = 1.4 \times 10^{-3}$ for evaporation) to compute the surface fluxes. These mean winds were reconstructed from the evaporation values in Thompson et al., the difference in q between the surface and the first model level (about 35 m above the surface) and a drag coefficient (appropriate to 35 m) of $C_D = C_E = 1.14 \times 10^{-3}$. This value of a drag coefficient was computed from the value used by Thompson et al (1979) assuming a log-wind profile:

$$C_D(35) = C_D(10) \left(\frac{\ell n(10/Z_o)}{\ell n(35/Z_o)}\right)^2$$

with $Z_o = 0.032\ u_*^2/g$, where $u_*$ is the friction velocity. Fig. 2.13 shows the observed surface fluxes and those computed with the boundary layer scheme, showing that the convection scheme and boundary layer diffusion scheme are

working together satisfactorily. Fig. 2.14 shows the computed structure at 80 hrs. Because the convection scheme is not used to adjust the surface layer, the boundary layer diffusion scheme generates a mixed layer between the first two levels.

## 3. SHALLOW CONVECTION

### 3.1 BOMEX data set

The shallow convection adjustment scheme was tested using constant convective and radiative forcing ($Q_1$, $Q_2$, $Q_R$) derived from the budget study of Holland and Rasmusson (1973). Fig. 2.15 shows the large-scale adiabatic terms and radiative cooling used as forcing. The data represent a 5-day mean.
A 15-level one dimensional model was integrated for 72 hrs to see the response of the convective adjustment to the prescribed large-scale forcing.

The model shallow convection scheme finds a cloud-top using a moist adiabat through a low level $\theta_E$, and a mixing line between cloud-base and one level above cloud-top. Cloud-base was kept fixed at $\sigma$-level 14 (about 980 mb). The temperature profile for the convective adjustment has the slope of this mixing line; the moisture profile has constant $\mathcal{P}$ . After correcting both temperature and moisture adjustment profiles to satisfy enthalpy and moisture conservation (Eqs. 17, 18) the convective adjustment is applied from the cloud-base level to cloud-top. The boundary layer diffusion scheme computes the fluxes at the surface and below cloud-base, and in so doing produces a shallow mixed layer.

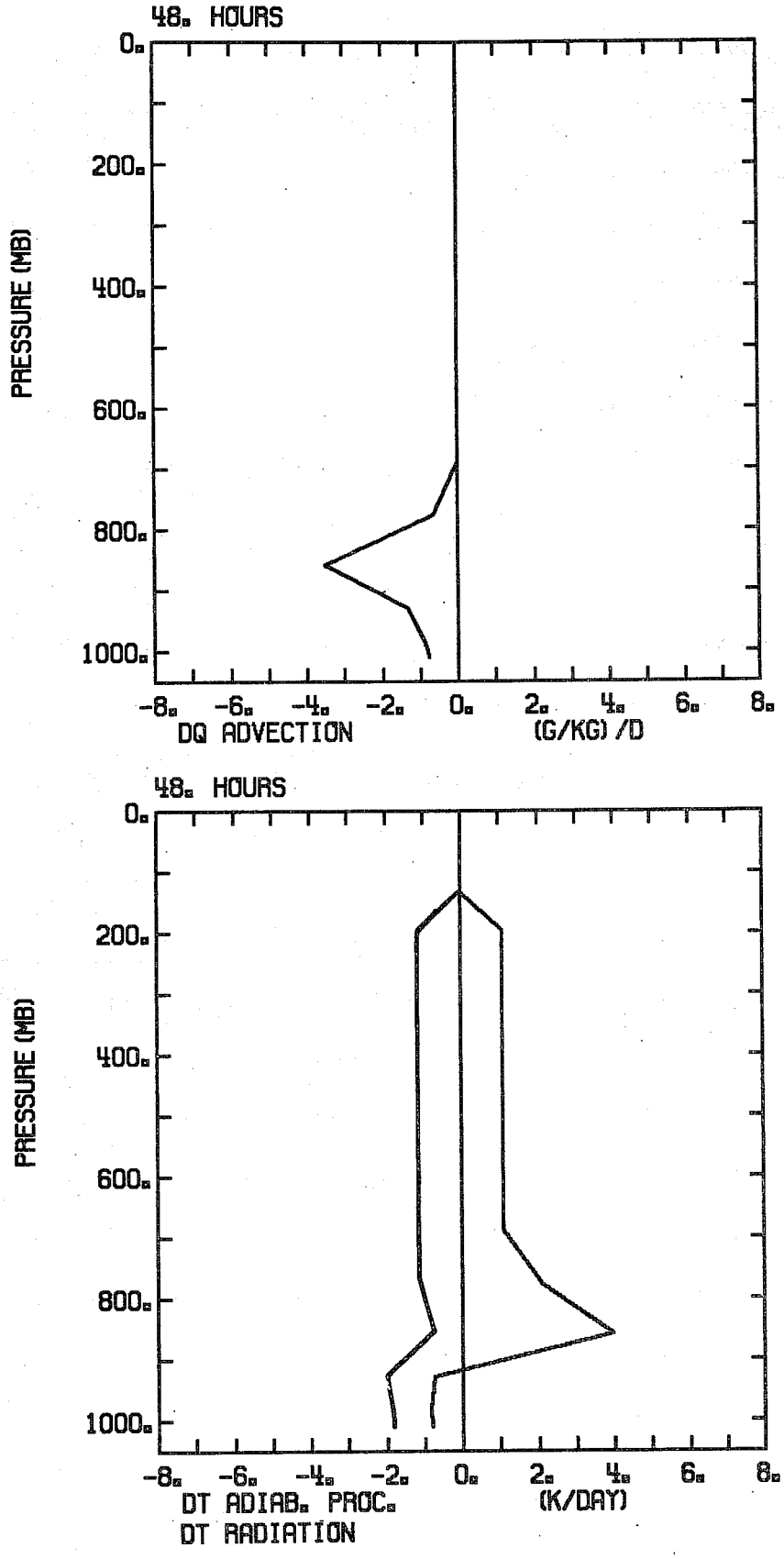


Fig. 2.15 BOMEX adiabatic and radiative forcing terms.

Fig. 2.16 shows the structure at 24 hrs produced by the convection scheme. It is in good agreement with the observed steady state structure although the simulation gives a moister boundary layer. This is probably realistic: further corrections were subsequently made to the BOMEX humidity data which increased the boundary layer specific humidity by 1-2 g $Kg^{-1}$ (Rasmusson, personal communication). The simulation is not quite in a steady state. The shallow convection scheme selects 850 mb as the level below cloud-top and makes no adjustment at 777 mb, the next model level which is above cloud-top. The adiabatic forcing at this level, though small (Fig. 2.15), is therefore unbalanced and the inversion strengthens with time, although the convection scheme maintains cloud-top at the same level. Fig. 2.17 shows the profiles of the parameterized heating and moistening and the boundary layer diffusion terms. It is the convective cooling at 850 mb which is crucial to the maintenance of the trade inversion at this height. In nature it is produced by the evaporation of overshooting cloud-tops (Betts, 1973): here the parametric scheme, by maintaining the temperature structure against the large-scale subsidence heating, is simulating the process. Neither the current ECMWF boundary layer scheme nor ECMWF's versions of Kuo or Arakawa and Schubert's parameterisations adequately reproduce this cooling below the trade inversion. The result is that the inversion collapses within 48 hrs towards the surface, the boundary layer saturates, and the surface evaporation is significantly reduced. The enhanced diffusion scheme (Tiedtke, 1983) does succeed in maintaining a realistic temperature structure up to the inversion.

The surface fluxes are given in Table 2.2 for different convective adjustment times, $\tau$.

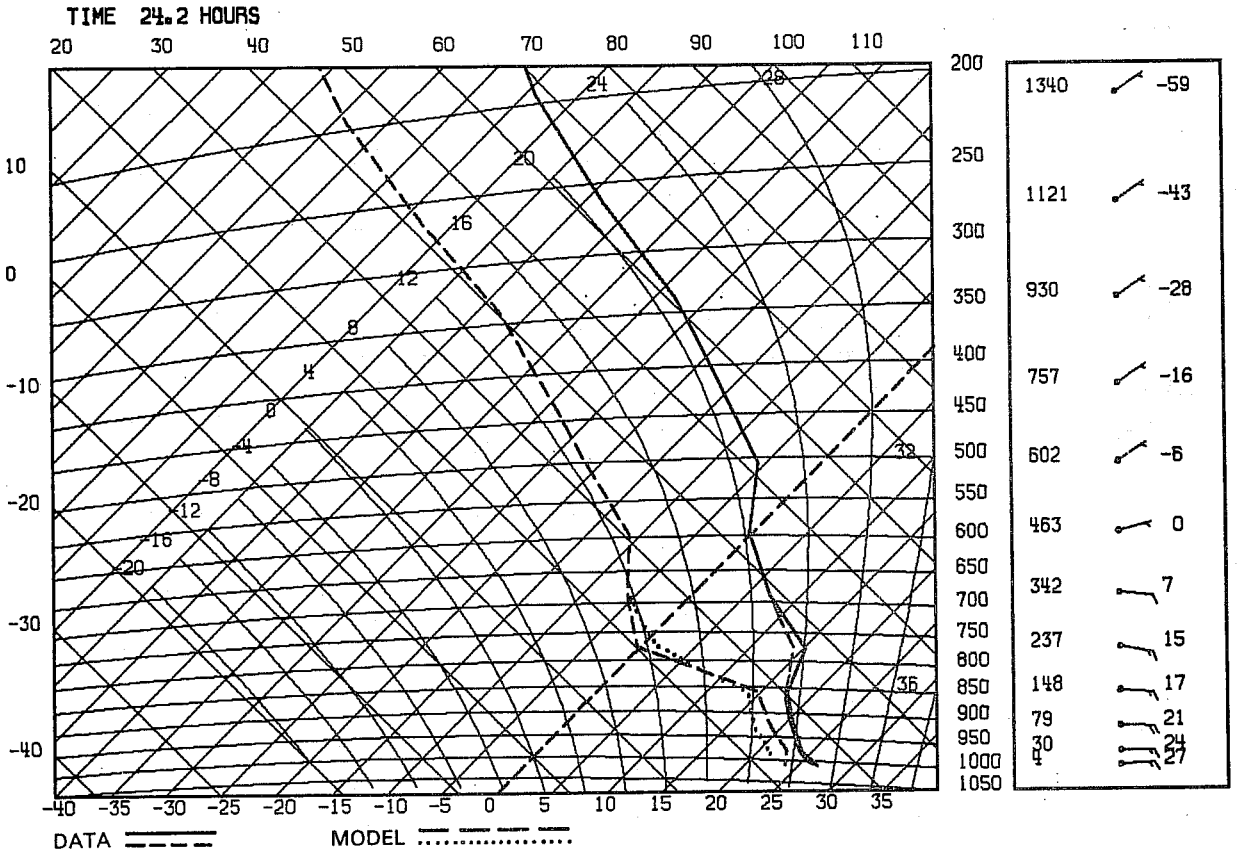


Fig. 2.16 Comparison of observed and model boundary layer structure for BOMEX using convective adjustment scheme.

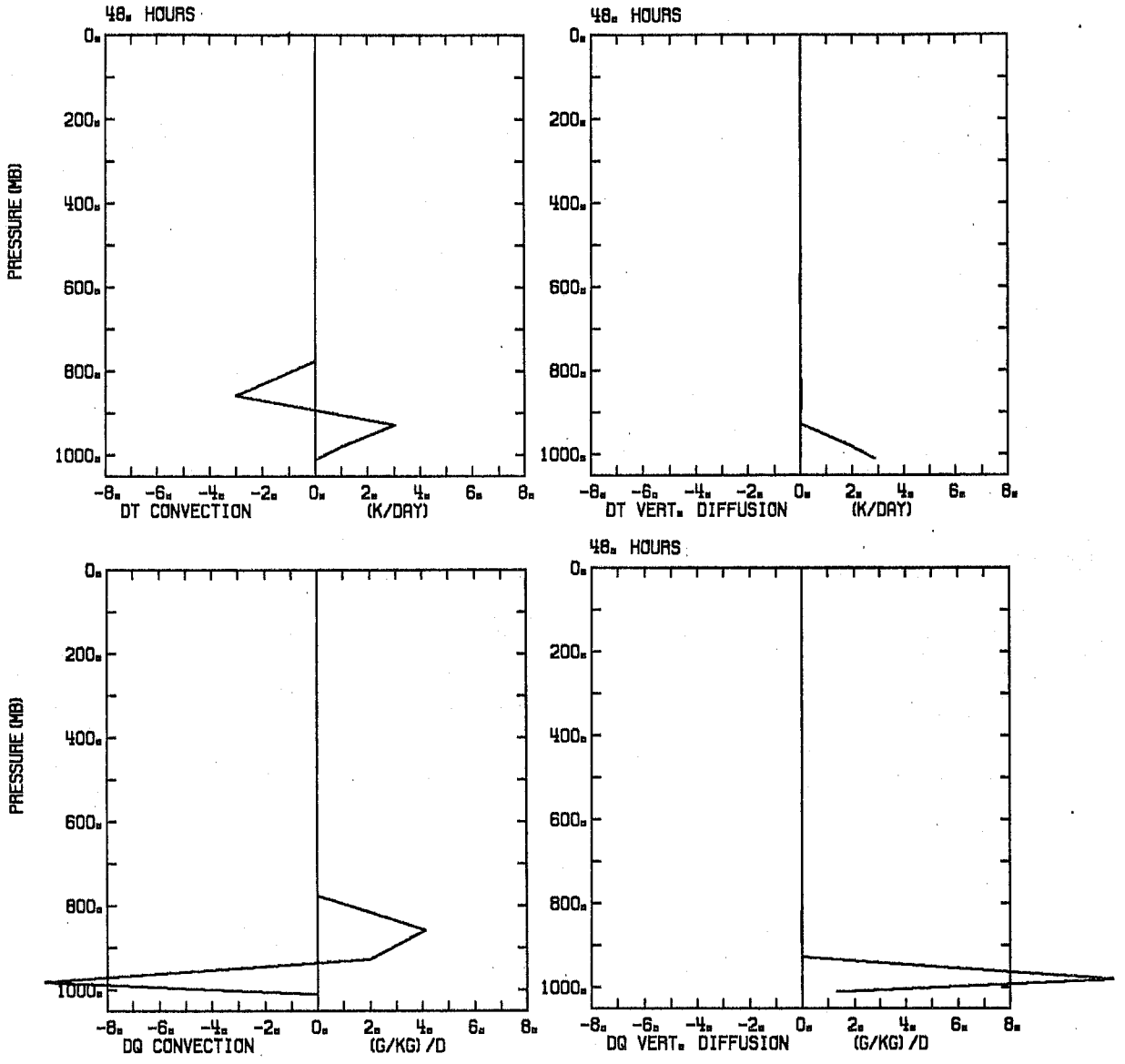


Fig. 2.17 Computed BOMEX convective source terms and boundary layer diffusion terms.

| | Model (48 hrs mean) | | | Observed Holland and Rasmusson (1973) | Units |
|---|---|---|---|---|---|
| $\tau$ | 1 | 2 | 3 | | hrs |
| Sensible heat flux | 17 | 17 | 16 | 15 | W $m^{-2}$ |
| Latent heat flux | 175 | 168 | 161 | 169 | W $m^{-2}$ |

Table 2.2 Comparison of observed and model surface fluxes for BOMEX

The agreement with observation is very good and the variation with the convective adjustment time-scale $\tau$ is small.

## 3.2 ATEX data set

The BOMEX tests were repeated for a similar data set derived from the Atlantic Trade wind Experiment (ATEX) (Augstein et al., 1973; Wagner, 1975) with very similar results. Fig. 2.18 shows the comparison of the model and the data (ATEX undisturbed period mean; 7-12 February 1969) at 24 hrs. The comparison is quite good. In this case, the model temperature profile is more stable than that observed. Fig. 1.9 also shows that the observed mixing line is somewhat more stable than the cloud layer temperature profile. However, the 'observed' vertical structure may be unrepresentative of horizontal averages because of the special procedure used to generate it (Augstein et al, 1973), which sharpens vertical gradients. In addition, in the model simulation, the mixed layer is too shallow compared with the observations, because of the limited model resolution in the boundary layer.

The model simulation maintains a similar temperature profile for 72 hrs with an adjustment time-scale $\tau$ = 2 hrs; although the inversion strengthens steadily as in the BOMEX case, because the large-scale advective terms are unbalanced slightly at 778 mb. Fig. 2.19 shows that the convective cooling below the inversion is again reproduced. With a faster adjustment time ($\tau$ = 1 hr) the same inversion height is maintained for 96 hrs, while for longer $\tau$ = 3 hrs), the inversion starts to fall in height about 60 hrs.

| | Model (48 hr mean) | | | Observed Krügermeyer (1975) | Units |
|---|---|---|---|---|---|
| $\tau$ | 1 | 2 | 3 | | hrs |
| Sensible heat flux | 12 | 12 | 13 | 14 | W $m^{-2}$ |
| Latent heat flux | 159 | 154 | 148 | 208 | W $m^{-2}$ |

Table 2.3 Comparison of observed model surface fluxes for ATEX

Table 2.3 compares the model surface fluxes with observed values (Krügermeyer, 1975). The model values vary little with adjustment time-scale $\tau$, but the computed latent heat fluxes are rather less than the value given by Krügermeyer (1975) for the undisturbed ATEX period average (which seems high).

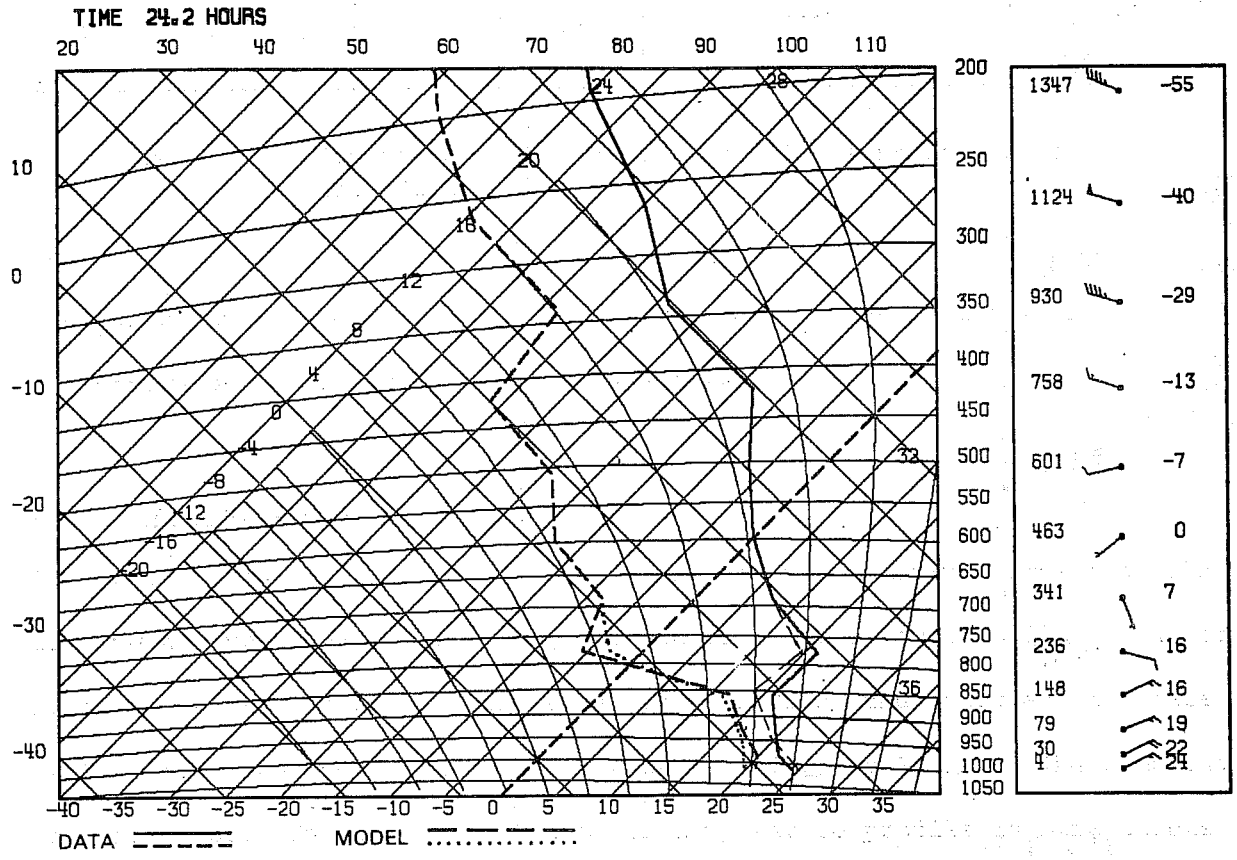


Fig. 2.18 As Fig. 2.16 for ATEX comparison.

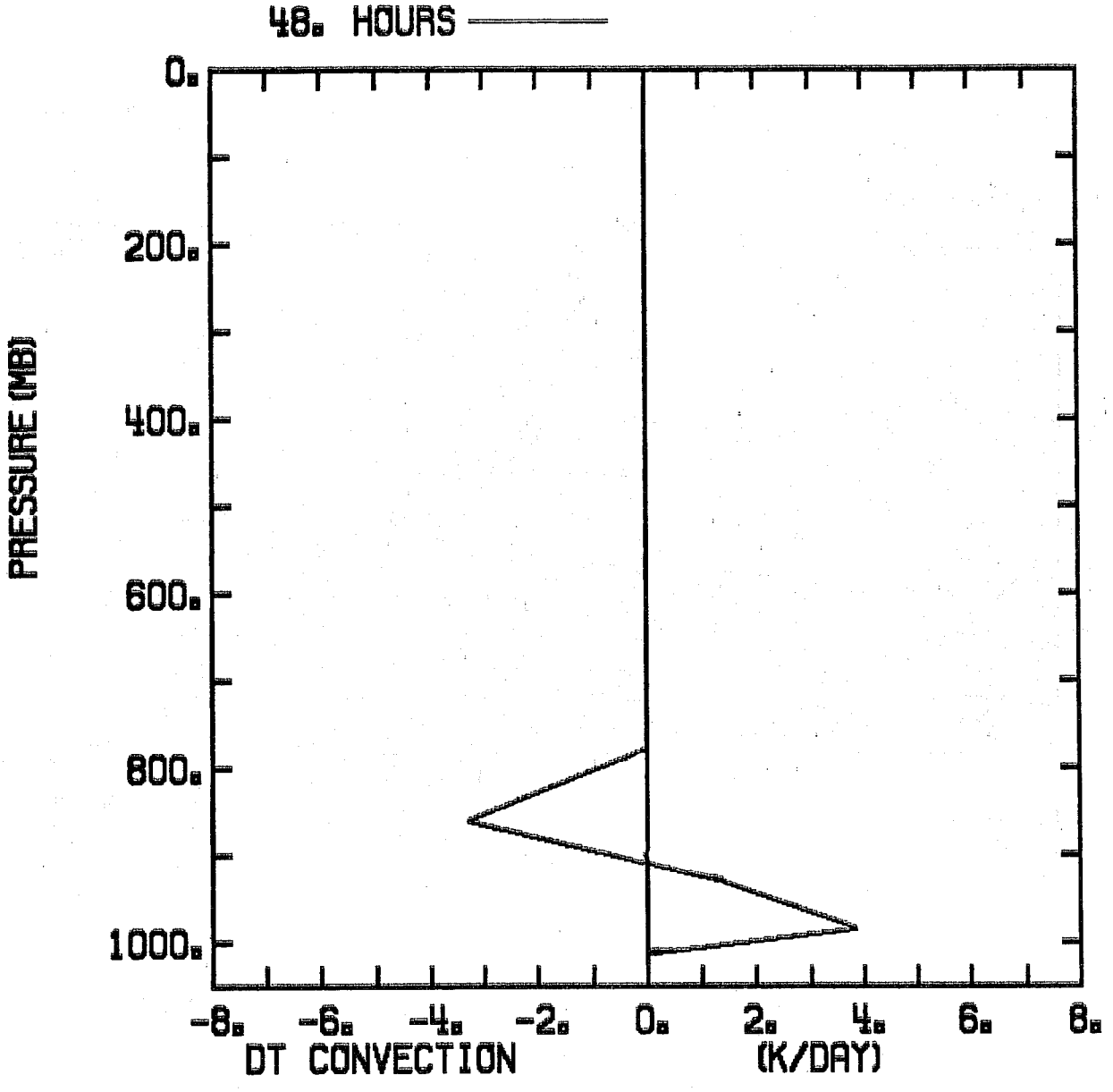


Fig. 2.10 Computed ATEX convective heat source.

## 4. ARCTIC AIR MASS TRANSFORMATION

Both shallow and deep convection schemes were tested using an Arctic air-mass data set (Økland, 1976). This case is discussed in Tiedtke, 1977. An initially cold sounding (observed) is advected southward at constant speed over a warmer ocean (with ocean temperatures increasing southward). The surface fluxes are very large and large-scale advective changes and radiation are neglected in comparison. The atmospheric structure after integration for 18 hrs along this mean southward trajectory is compared with an observed sounding.

In the simulation the shallow convection scheme operates first and the boundary layer deepens, saturates, giving some large-scale precipitation, until the deep convection scheme is activated when cloud-top reaches above model level 11 at 765 mb. Convective precipitation replaces large-scale precipitation and the final structure at 18 hrs compared to the observed structure (a single sounding) is shown in Fig. 2.20 (using adjustment timescale $\tau$ = 2 hrs). The agreement is reasonable considering large-scale advective terms have been neglected. The observed sounding with a lifting condensation level at 890 mb seems too dry at the surface. The convection top has reached 600 mb by 18 hrs. Fig. 2.21 shows the sensible and latent heat fluxes at the surface; Fig. 2.22 the large-scale and convective scale precipitation.

The simulation was also repeated specifying a different cloud-top level for the transition from shallow non-precipitating to deep convection. Allowing convective precipitation from shallow clouds (tops above model level 12 at 845 mb)reduced the large-scale precipitation, and increased the convective precipitation but did not change the structure at 18 hrs. On the other hand, if convective precipitation was suppressed until cloud-top was higher

(above model layer 10 at 678 mb) the atmosphere is saturated with only large-scale precipitation at 18 hrs (Fig. 2.23). The 18 hr mean surface fluxes, however, only change slightly as the shallow convection transition height is changed. Table 2.4 summarises the surface energy fluxes for $\tau$ = 2 hrs.

| Cloud top limit for | 12 | 11 | 10 | model level |
|---|---|---|---|---|
| no convective precipitation | 845 | 765 | 678 | mb |
| Sensible heat flux | 230 | 234 | 241 | W $m^{-2}$ |
| Latent heat flux | 191 | 188 | 187 | W $m^{-2}$ |
| Total heat flux | 421 | 422 | 428 | W $m^{-2}$ |
| Large-scale precipitation | 12 | 32 | 60 | W $m^{-2}$ |
| Convective precipitation | 74 | 51 | 0 | W $m^{-2}$ |
| Total precipitation | 86 | 83 | 60 | W $m^{-2}$ |

Table 2.4

The interaction of the shallow convective scheme and large-scale precipitation scheme seems satisfactory. Without convective precipitation, the boundary layer saturates with the large surface fluxes. The shallow convection-scheme steadily deepens the saturated boundary layer, while the large-scale precipitation scheme removes supersaturation, simulating a deepening strato-cumulus layer. Once cloud-tops reach a sufficient height, the transition to convective precipitation dries out the boundary layer.

These runs were repeated for different adjustment time-scales ($\tau$ = 1 and 3 hrs) with similar results.

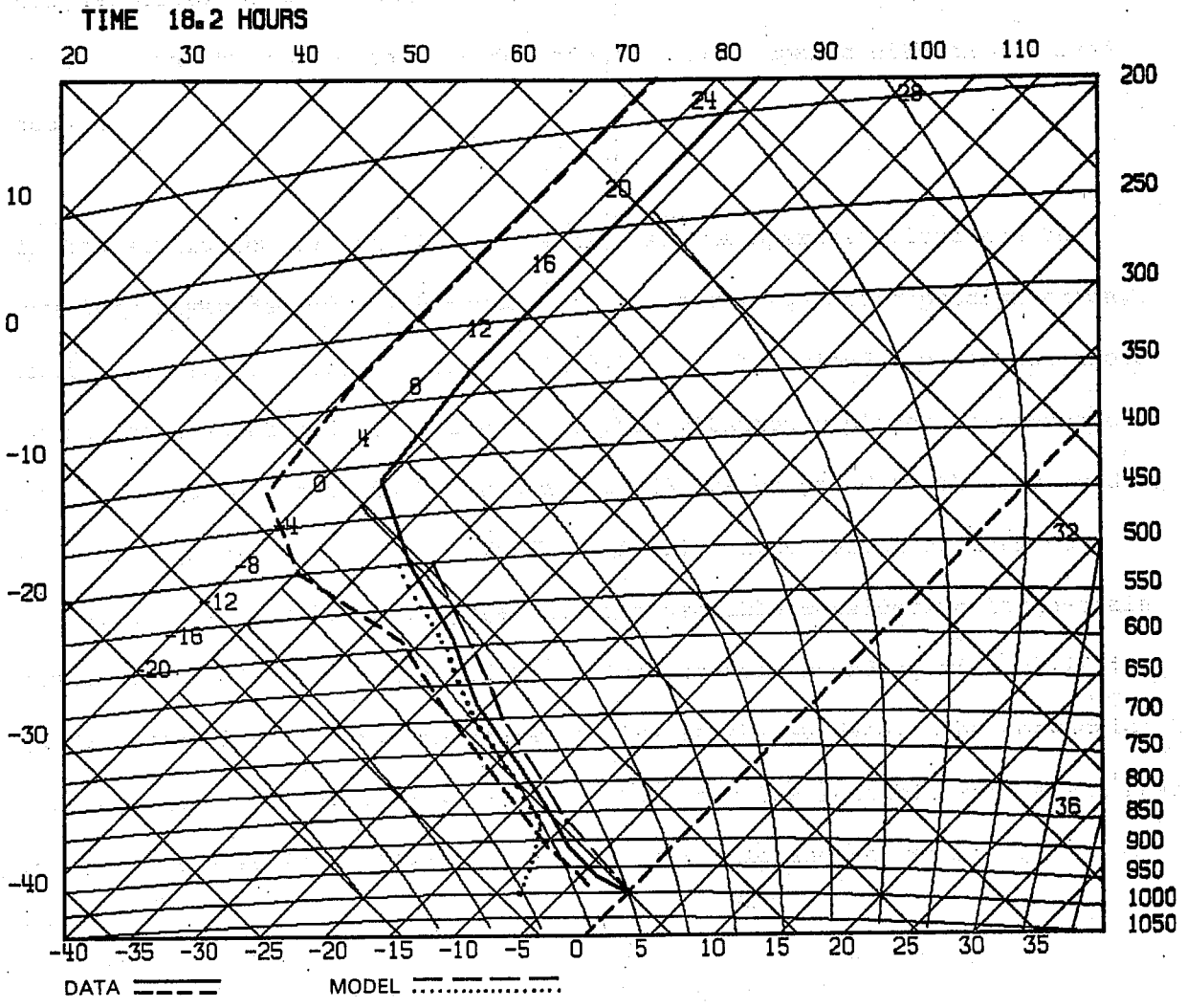


Fig. 2.20 Comparison of observed and model structure after integration for 18 hrs along a southerly trajectory for an Arctic airmass transformation.

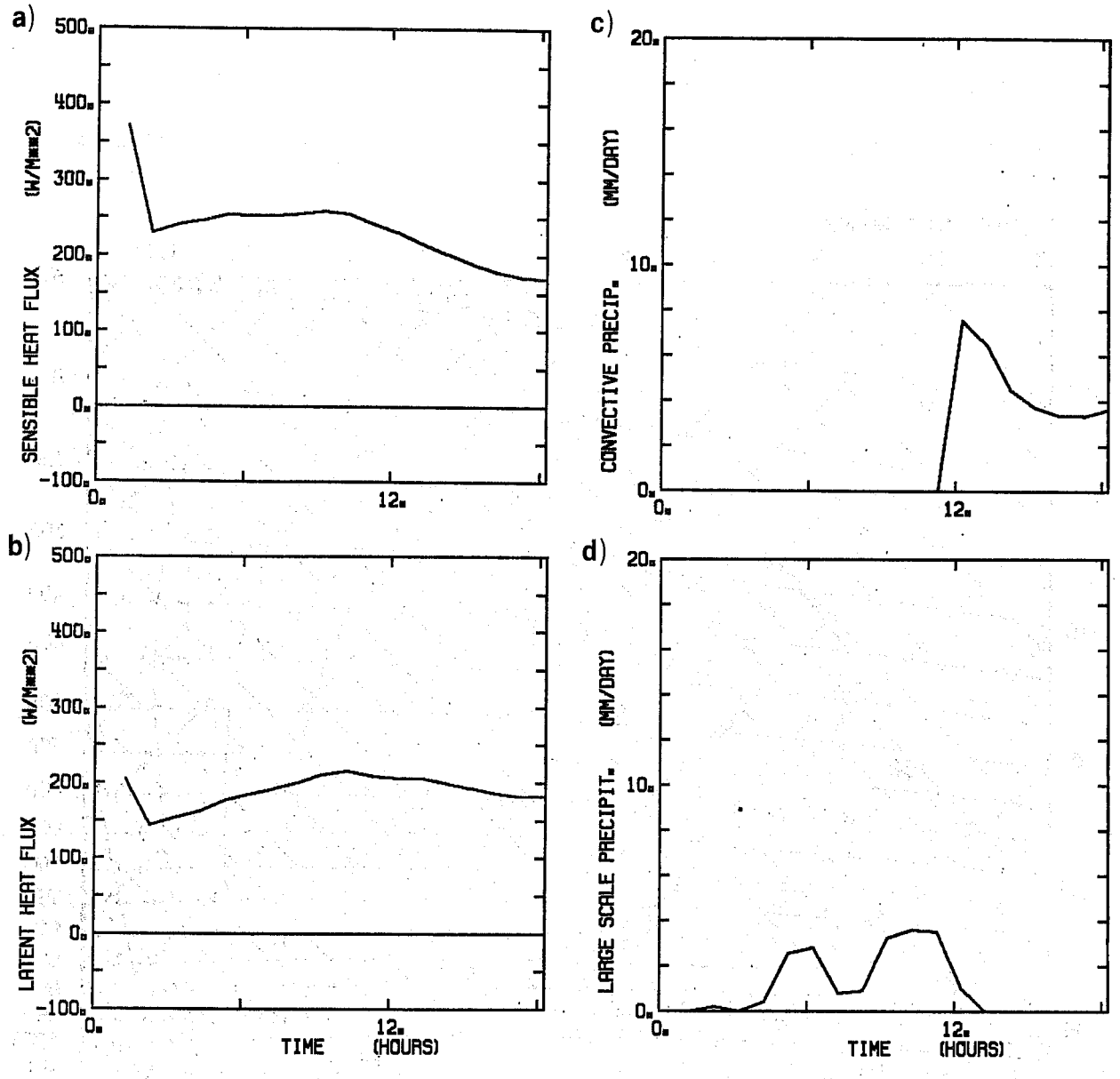


Fig. 2.21 a) sensible and b) latent heat fluxes c) convective and d) large-scale precipitation for the Arctic airmass transformation.

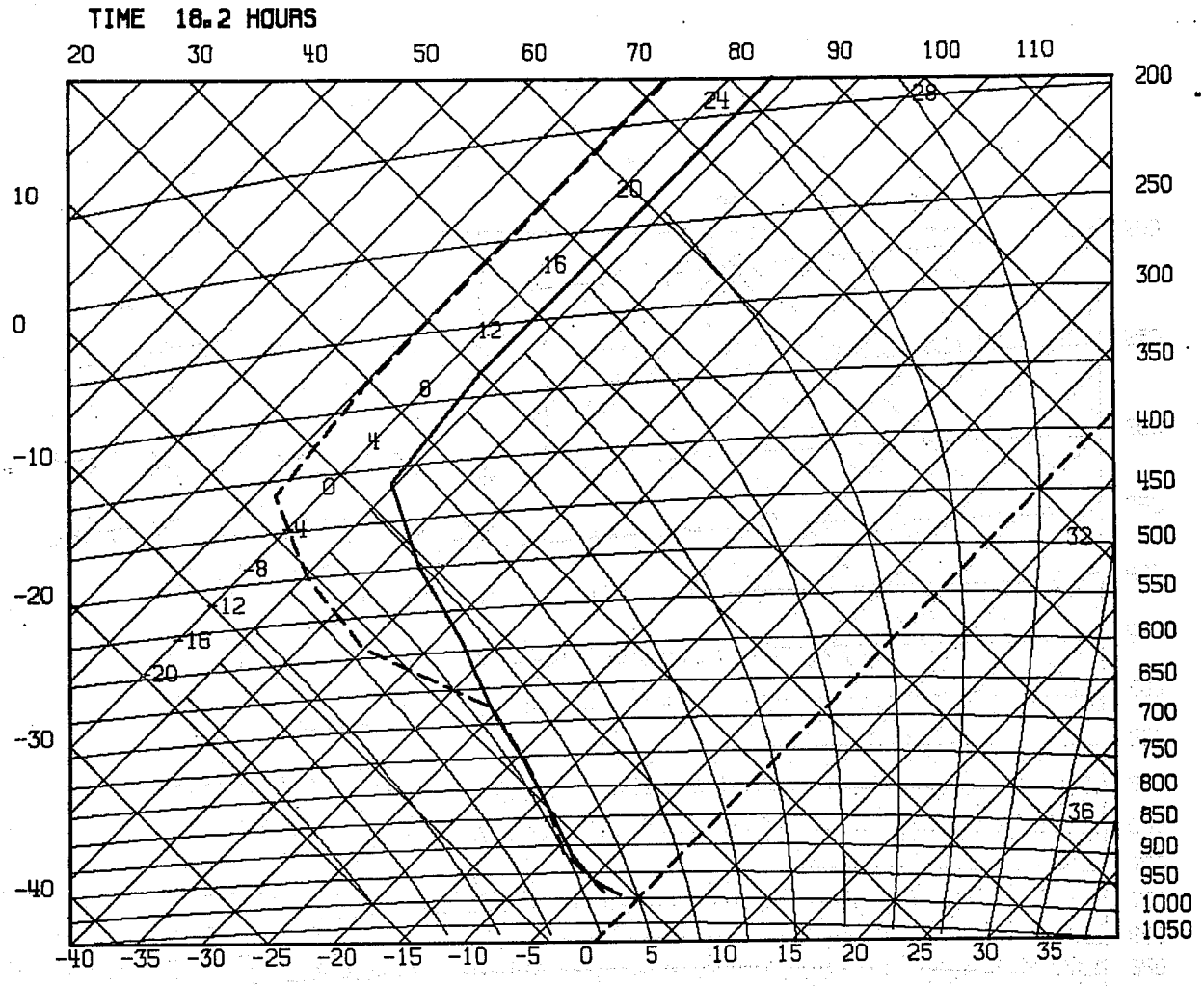


Fig. 2.22 Model structure at 18 hrs with only shallow convection scheme operating.

CONCLUDING REMARKS

These parameter schemes for deep and shallow convection were then introduced into the N48 gridpoint model for one and ten-day test forecasts, where they appeared to perform well. These studies and the adaptation of the scheme to the current spectral model are still in progress, but the initial results are summarised here. The first 10-day forecast using this convection scheme shows significant changes in global climatic parameters when compared with the standard forecast using Kuo's scheme: see Table 2.1.

Table 2.1 Difference in 6-10 day global means between this parametric scheme and Kuo's scheme [10-day forecast initial date - June 11, 1979].

| | |
|---|---|
| Tropical mean temperature | + 2K |
| Global latent heat flux | + 24% |
| Global sensible heat flux | + 18% |
| Global convective precipitation | + 16% |
| Global large-scale precipitation | + 7% |

It is clear that the shallow convection scheme is primarily responsible for these changes. By transporting moisture upward out of the subcloud layer over the tropical oceans, the surface latent heat flux increases, increasing the global precipitation and reducing the tendency (seen with Kuo's scheme) for the model atmosphere to cool with time. These changes are so large that the difference between this deep convection scheme and Kuo's are not immediately visible.

Acknowledgements

This research was completed while one author (AKB) was a Visiting Scientist at ECMWF. The theoretical part of this work was supported by the National Science Foundation under grant ATM81-20444.

References

Arakawa, A. and W.H. Schubert 1974: Interaction of a cumulus cloud ensemble with the large-scale environment: Part I. J.Atmos.Sci., 31, 674-701.

Albrecht, B.A., A.K. Betts, W.H. Schubert and S.K. Cox 1979: A model of the thermodynamic structure of the trade-wind boundary layer: Part I. Theoretical formulation and sensitivity tests. J.Atmos.Sci., 36, 73-89.

Augstein, E., H. Riehl, F. Ostopoff, and V. Wagner 1973: Mass and energy transports in an undisturbed Atlantic trade-wind flow. Mon.Wea.Rev., 101, 101-111.

Betts, A.K. 1973: Non-precipitating cumulus convection and its parameterization. Quart.J.Roy.Meteor.Soc., 99, 178-196.

Betts, A.K. 1974: The scientific basis and objectives of the US Convection Subprogram for the GATE. Bull.Amer.Met.Soc., 55, 304-313.

Betts, A.K. 1978: Convection in the tropics. Meteorology over the tropical oceans, D.B. Shaw, Roy.Meteor.Soc., 105-132.

Betts, A.K. 1982a: Saturation point analysis of moist convective overturning. J.Atmos.Sci., 39, 1484-1505.

Betts, A.K. 1982b: Cloud thermodynamic models in saturation point coordinates. J.Atmos.Sci., 39, 2182-2191.

Betts, A.K. 1983a: Thermodynamics of mixed stratocumulus layers: saturation point budgets. J.Atmos.Sci., 40, 2655-2670.

Betts, A.K. 1983b: Atmospheric convective structure and a convection scheme based on saturation point adjustment. Workshop on convection in large-scale models. 28 Nov.-1 Dec. 1983 (to be published).

Barnes, G.M. and K. Sieckman 1984: The environment of fast and slow tropical mesoscale convective cloud lines. Mon.Wea.Rev. (to be published).

Cox, S.K. and K.T. Griffith 1979: Estimates of radiative flux divergence during Phase III of the GARP Atlantic Tropical Experiment, Part II: Analysis of Phase III results. J.Atmos.Sci., 36, 586-601.

Frank, W.M. 1977: The structure and energetics of the tropical cyclone, Part I: Storm structure. Mon.Wea.Rev., 105, 1119-1135.

Frank, W.M. 1978: The life-cycles of GATE convective systems. J.Atmos.Sci., 35, 1256-1264.

Frank, W.M. 1983: The cumulus parameterization problem. Mon.Wea.Rev., 111, 1859-1871.

Holland, J.Z. and E.M. Rasmusson 1973: Measurements of the atmospheric mass, energy and momentum budgets over a 500 km square of tropical ocean. Mon.Wea.Rev., 101, 44-55.

Houze, R.A. and A.K. Betts 1981: Convection in GATE. Rev.Geophys.Space Phys., 19, 541-576.

Kuo, H.L. 1965: On formation and intensification of tropical cyclones through latent heat release by cumulus convection. J.Atmos.Sci., 22, 40-63.

Kuo, H.L. 1974: Further studies of the parameterization of the influence of cumulus convection of large-scale flow. J.Atmos.Sci., 31, 1232-1240.

Krügermeyer, L. 1975: Vertical transports of momentum, sensible and latent heat from profiles at the tropical Atlantic during ATEX. Berichte Inst. Radiometeor. und Maritime Meteor., Univ. Hamburg, No.29, 77pp. (in German).

Lord, S.J. 1982: Interaction of a cumulus cloud ensemble with the large-scale environment. Part III: Semi-prognostic test of the Arakawa-Schubert cumulus parameterization. J.Atmos.Sci., 39, 88-103.

Lord, S.J. and A. Arakawa 1980: Interaction of a cumulus ensemble with the large-scale environment. Part II. J.Atmos.Sci., 37, 2677-2692.

Manabe, S. J. Smagorinsky and R.F. Strickler 1965: Simulated climatology of a general circulation model with a hydrologic cycle. Mon.Wea.Rev., 93, 769-798.

Ooyama, K. 1971: A theory of parameterisation of cumulus convection. J.Meteor.Soc.Japan, 49, 744-756.

Økland, H. 1976: An example of air-mass transformation in the Arctic and convective disturbances of the windfield. Report DM-20, Univ. of Stockholm., 30pp.

Thompson Jr., R.M., S.W. Payne, E.E. Reckel and R.J. Reed 1979: Structure and properties of synoptic-scale wave disturbances in the intertropical convergence zone of the eastern Atlantic. J.Atmos.Sci., 36, 53-72.

Tiedtke, M. 1977: Numerical tests of parameterisation schemes at an actual case of transformation of Arctic air. ECMWF Internal Report No.10, 21pp.

Tiedtke, M. 1983: The sensitivity of the time-mean large-scale flow to cumulus convection in the ECMWF model. ECMWF Workshop on Convection in Large-scale Models, 28 Nov.-1 Dec. 1983 (to be published).

Wagner, V. 1975: Relationships between the tropospheric circulation and energetic processes within the Hadley circulation over the Atlantic Ocean. Berichte Inst. Radiometeor. und Maritime Meteor. Univ. Hamburg, No.26, 83pp.

Zipser, E.J. and M.A. LeMone 1980: Cumulonimbus vertical velocity events in GATE Part II: Synthesis and model core structure. J.Atmos.Sci., 37, 2458-2469.

ECMWF PUBLISHED TECHNICAL REPORTS

No.1 A Case Study of a Ten Day Prediction

No.2 The Effect of Arithmetic Precisions on some Meteorological Integrations

No.3 Mixed-Radix Fast Fourier Transforms without Reordering

No.4 A Model for Medium-Range Weather Forecasting - Adiabatic Formulation

No.5 A Study of some Parameterizations of Sub-Grid Processes in a Baroclinic Wave in a Two-Dimensional Model

No.6 The ECMWF Analysis and Data Assimilation Scheme - Analysis of Mass and Wind Fields

No.7 A Ten Day High Resolution Non-Adiabatic Spectral Integration: A Comparative Study

No.8 On the Asymptotic Behaviour of Simple Stochastic-Dynamic Systems

No.9 On Balance Requirements as Initial Conditions

No.10 ECMWF Model - Parameterization of Sub-Grid Processes

No.11 Normal Mode Initialization for a Multi-Level Gridpoint Model

No.12 Data Assimilation Experiments

No.13 Comparisons of Medium Range Forecasts made with two Parameterization Schemes

No.14 On Initial Conditions for Non-Hydrostatic Models

No.15 Adiabatic Formulation and Organization of ECMWF's Spectral Model

No.16 Model Studies of a Developing Boundary Layer over the Ocean

No.17 The Response of a Global Barotropic Model to Forcing by Large-Scale Orography

No.18 Confidence Limits for Verification and Energetic Studies

No.19 A Low Order Barotropic Model on the Sphere with the Orographic and Newtonian Forcing

No.20 A Review of the Normal Mode Initialization Method

No.21 The Adjoint Equation Technique Applied to Meteorological Problems

No.22 The Use of Empirical Methods for Mesoscale Pressure Forecasts

No.23 Comparison of Medium Range Forecasts made with Models using Spectral or Finite Difference Techniques in the Horizontal

No.24 On the Average Errors of an Ensemble of Forecasts

ECMWF PUBLISHED TECHNICAL REPORTS

No.25 On the Atmospheric Factors Affecting the Levantine Sea

No.26 Tropical Influences on Stationary Wave Motion in Middle and High Latitudes

No.27 The Energy Budgets in North America, North Atlantic and Europe Based on ECMWF Analyses and Forecasts

No.28 An Energy and Angular-Momentum Conserving Vertical Finite-Difference Scheme, Hybrid Coordinates, and Medium-Range Weather Prediction

No.29 Orographic Influences on Mediterranean Lee Cyclogenesis and European Blocking in a Global Numerical Model

No.30 Review and Re-assessment of ECNET - a Private Network with Open Architecture

No.31 An Investigation of the Impact at Middle and High Latitudes of Tropical Forecast Errors

No.32 Short and Medium Range Forecast Differences between a Spectral and Grid Point Model. An Extensive Quasi-Operational Comparison

No.33 Numerical Simulations of a Case of Blocking: the Effects of Orography and Land-Sea Contrast

No.34 The Impact of Cloud Track Wind Data on Global Analyses and Medium Range Forecasts

No.35 Energy Budget Calculations at ECMWF: Part I: Analyses

No.36 Operational Verification of ECMWF Forecast Fields and Results for 1980-1981

No.37 High Resolution Experiments with the ECMWF Model: a Case Study

No.38 The Response of the ECMWF Global Model to the El-Nino Anomaly in Extended Range Prediction Experiments

No.39 On the Parameterization of Vertical Diffusion in Large-Scale Atmospheric Models

No.40 Spectral characteristics of the ECMWF Objective Analysis System

No.41 Systematic Errors in the Baroclinic Waves of the ECMWF Model

No.42 On Long Stationary and Transient Atmospheric Waves

No.43 A New Convective Adjustment Scheme